Determinants of *de novo* B cell responses to drifted epitopes in post-vaccination SARS-CoV-2 infections

Grace E. Quirk[1,*], Marta V. Schoenle[2,*,^], Kameron L. Peyton[2], Jennifer L. Uhrlaub[2], Branden Lau[3], Jefferey L. Burgess[4], Katherine Ellingson[5], Shawn Beitel[4], James Romine[4], Karen Lutrick[6], Ashley Fowlkes[7], Amadea Britton[7], Harmony L. Tyner[8], Alberto J. Caban-Martinez[9], Allison Naleway[10], Manjusha Gaglani[11], Sarang Yoon[12], Laura Edwards[13], Lauren Olsho[13], Michael Dake[14], Bonnie J. LaFleur[15], Janko Ž. Nikolich[,15,16], Ryan Sprissler[3], Michael Worobey[1,15,#], and Deepta Bhattacharya[2,15,17,#]

[1] Department of Ecology and Evolutionary Biology, University of Arizona, Tucson, AZ, USA

[2]Department of Immunobiology, University of Arizona College of Medicine, Tucson, AZ, USA

[3] University of Arizona Genomics Core and the Arizona Research Labs, University of Arizona Genetics Core, University of Arizona, Tucson, AZ, USA

[4] Mel and Enid Zuckerman College of Public Health, University of Arizona, Tucson, Arizona, USA

[5] Department of Epidemiology and Biostatistics, Zuckerman College of Public Health, University of Arizona, Tucson

[6] College of Medicine-Tucson, University of Arizona, Tucson, Arizona, USA

20 [7] National Center for Immunization and Respiratory Diseases, Centers for Disease
21 Control and Prevention, Atlanta, GA

22 [8] St. Luke's Regional Health Care System, Duluth, Minnesota, USA

23 [9] University of Miami, Leonard M. Miller School of Medicine, Miami, FL, USA

24 [10] Kaiser Permanente Northwest Center for Health Research, Portland, Oregon, USA

25 [11] Baylor Scott & White Health and Texas A&M University College of Medicine, Temple,
26 Texas, USA

27 [12] Rocky Mountain Center for Occupational and Environmental Health, Department of
28 Family and Preventive Medicine, University of Utah Health, Salt Lake City, Utah, USA

29 [13] Abt Associates, Rockville, Maryland, USA

30 [14] Office of the Senior Vice-President for Health Sciences, University of Arizona,
31 Tucson, AZ, USA

32 [15] BIO5 Institute, University of Arizona, Tucson, AZ, USA

33 [16] University of Arizona Center on Aging, University of Arizona College of Medicine,
34 Tucson, AZ, USA

35 [17] Department of Surgery, University of Arizona College of Medicine, Tucson, AZ, USA

36 *These authors contributed equally

37 #These authors contributed equally

38 ^Current address: Department of Microbiology and Immunology, Cornell University,

39 Ithaca, NY

40 Address correspondence to: deeptab@arizona.edu

Summary:
Vaccine-induced immunity may impact subsequent *de novo* responses to drifted epitopes in SARS-CoV-2 variants, but this has been difficult to quantify due to the challenges in recruiting unvaccinated control groups whose first exposure to SARS-CoV-2 is a primary infection. Through local, statewide, and national SARS-CoV-2 testing programs, we were able to recruit cohorts of individuals who had recovered from either primary or post-vaccination infections by either the Delta or Omicron BA.1 variants. Regardless of variant, we observed greater Spike-specific and neutralizing antibody responses in post-vaccination infections than in those who were infected without prior vaccination. Through analysis of variant-specific memory B cells as markers of *de novo* responses, we observed that Delta and Omicron BA.1 infections led to a marked shift in immunodominance in which some drifted epitopes elicited minimal responses, even in primary infections. Prior immunity through vaccination had a small negative impact on these *de novo* responses, but this did not correlate with cross-reactive memory B cells, arguing against competitive inhibition of naïve B cells. We conclude that dampened *de novo* B cell responses against drifted epitopes are mostly a function of altered immunodominance hierarchies that are apparent even in primary infections, with a more modest contribution from pre-existing immunity, perhaps due to accelerated antigen clearance.

60 **Introduction:**

61 Within a year of the discovery of SARS-CoV-2 as the etiological agent of COVID-
62 19[1], highly effective vaccines were developed and administered. Leading this class
63 were the monovalent mRNA vaccines BNT162b2 and mRNA-1273 encoding the
64 ancestral Spike protein, both of which achieved ~95% efficacies in preventing
65 symptomatic illness[2,3]. Other vaccine platforms also achieved high efficacies, especially
66 against severe illness and hospitalization[4–8]. Since the initial results of these clinical
67 trials, however, the protective capacity of these vaccines has declined[9–12]. This drop in
68 vaccine effectiveness is due to both waning of antibodies and viral evolution and escape
69 from vaccine-induced neutralizing antibodies, which are the best-known correlates of
70 protection[13,14]. While the known genetic diversity of SARS-CoV-2 was quite modest
71 through most of 2020[15], new variants with enhanced transmissibility and/or neutralizing
72 antibody escape mutations have since emerged and sequentially swept to global
73 dominance[12,16–24]. As of this writing, the dominant circulating variant is Omicron, which
74 comprises sublineages that contain Spike protein mutations located within most known
75 neutralizing antibody epitopes[25]. A key issue that will define both protection against
76 infections and the strategy underlying updates to the vaccines is the extent to which
77 pre-existing vaccine-induced immunity protects against heterologous challenges like
78 Omicron.

79 B cell responses following mRNA COVID-19 vaccination are characterized by
80 exceptionally long-lived germinal center reactions that persist for months while
81 continuously improving the breadth and affinity of antibodies[26–29]. Cells exiting the
82 germinal center carry affinity-enhancing mutations and can become long-lived antibody-

83 secreting plasma cells or memory B cells[30]. Depending on the subset of memory B cell,
84 re-exposures to antigen trigger differentiation to new plasma cells or germinal center
85 reactions[31–34]. After antigens from infection or vaccine antigens have been cleared,
86 long-lived plasma cells and memory B cells persist to maintain humoral immunity.
87 While these features protect against homologous SARS-CoV-2 infections, it is
88 more difficult to predict the nature of responses to subsequent heterologous infections
89 or vaccines. Due to their expanded pre-existing numbers and intrinsic signaling and
90 transcriptional differences relative to naive B cells, memory B cells rapidly mount
91 responses that are of greater magnitude than those of naïve primary responses[35–40] to
92 either initial infection or vaccination. Because of these properties, memory B cells that
93 react to epitopes conserved between the original and secondary challenges could
94 dominate the response to heterologous infections or vaccines[41–43]. If antigen and T cell
95 help are limiting, memory B cells might then outcompete naive B cells and new primary
96 antibody responses aimed at the new variant-specific epitopes. This phenomenon,
97 known as antigenic imprinting or “original antigenic sin”[44], can be beneficial if antibodies
98 against the conserved epitopes are protective. However, recall responses to
99 heterologous pathogens can potentially be neutral or even detrimental if antibodies
100 targeting these conserved epitopes are not protective and variant-specific primary
101 responses are competitively inhibited[45]. As an example of the phenomenon, pre-existing
102 common coronavirus-specific memory B cells compose a majority of the early response
103 to SARS-CoV-2, but primary responses to epitopes unique to SARS-CoV-2 are readily
104 observed later[26,46,47]. Whether common coronavirus immunity is helpful, harmful, or
105 neutral for *de novo* responses to SARS-CoV-2 is unknown.

106 In influenza infections, antigenic imprinting has been proposed to explain the
107 age-associated differential in morbidity and mortality based on influenza subtype
108 exposure history[48–51]. The various hemagglutinin (HA) subtypes of influenza A virus fall
109 into one or the other of two phylogenetically distinct HA “groups” (group 1 or group 2).
110 Individuals have the highest antibody titers against influenza strains encountered early
111 in life, and they experience enhanced protection against influenza strains that are within
112 the same HA group as their primary infection strain compared to heterosubtypic
113 infections from the group that is mismatched to their first childhood infection. Previous
114 work has shown that childhood exposure to H1N1 (group 1 hemagglutinin (HA)) affords
115 protection against other group 1 HAs, such as H5N1. The same is true for individuals
116 with group 2 HAs, whereby childhood H3N2 infection affords protection against H7N9.
117 Conversely, individuals with group 1 imprinting experience an increase in mortality when
118 faced with a group 2 influenza virus infection, such as that observed for H7N9
119 infections[48,51].
120 Though pre-existing immunity can certainly impact primary responses to
121 heterologous antigens, other mechanisms can also limit antibody responses to drifted
122 epitopes. Epitopes that were previously immunodominant for antibody responses do not
123 necessarily remain so once mutated, irrespective of prior immunity[52]. There are several
124 possible mechanistic reasons why not all epitopes are equal for antibody responses.
125 Factors such as naïve antigen-specific B cell precursor frequency and avidity vary
126 greatly across epitopes, which in turn correlate with their relative contribution to the
127 subsequent response[53–57]. Some epitopes can also be biophysically challenging for
128 antibody binding, such as those sterically blocked by glycan shields or appearing as

129 non-complex ‘smooth’ surfaces to B cells[58,59]. Further, epitopes that mimic self-antigens
130 also elicit poor responses due to tolerance mechanisms that remove or hamper B cells
131 from the repertoire that could otherwise respond[60–63]. Finally, V gene usage during
132 V(D)J recombination that gives rise to B cell receptors is uneven, as some segments
133 are more heavily utilized than others[64,65]. In turn, this can create ‘holes’ in the repertoire,
134 rendering some epitopes poorly immunogenic[66]. As SARS-CoV-2 variants of concern
135 accumulate mutations in antigenic regions, immunodominance might change in ways
136 that limit responses to drifted epitopes, with or without prior immunity. Thus, it has
137 remained difficult to examine the degree to which infrequent *de novo* variant-specific
138 responses in post-vaccination infections and heterologous boosters are due to changes
139 in immunodominance, antigenic imprinting, or some combination of both[67–75].
140 Antigenic imprinting has remained nearly impossible to quantify directly and
141 instead has predominantly relied on historical epidemiological data to make inferences
142 about biological mechanisms that produce the documented patterns[48,76,77]. The COVID-
143 19 pandemic presents a unique opportunity to address these questions: it has
144 encompassed adults with known infection histories and monovalent vaccines that
145 induce well characterized B cell responses[78–81] and the emergence of antigenically
146 distinct viral variants[25,82]. Yet, as immunological histories become more complex and
147 with very few immunologically naïve adults remaining[83,84], the Omicron BA.1 (BA.1, for
148 short) wave likely represented the final opportunity to recruit robust cohorts of
149 individuals that meet the key experimental and control criteria. Through voluntary saline-
150 gargle PCR testing of University of Arizona students, staff, and faculty as part of COVID
151 mitigation efforts on campus from August 2020 to July 2023; serological testing at 17

152 University of Arizona-managed sites across the state of Arizona; and two CDC-funded
153 cohorts of essential workers, Arizona Healthcare, Emergency Response, and Other
154 Essential Workers Surveillance (AZ HEROES)[85] and Research on Epidemiology of
155 SARS-CoV-2 in Essential Response Personnel (RECOVER)[86], we recruited
156 unvaccinated individuals who had recovered from primary Delta (B.1.617.2 or
157 B.1.617.2-like) or BA.1 (B.1.1.529 or B.1.1.529-like) infections. These cohorts allowed
158 us to characterize the immunodominance hierarchies for both Delta and BA.1 variants
159 and directly compare the specificity of antibody responses in unvaccinated individuals
160 infected by the antigenically drifted viral variants to those generated by post-vaccination
161 infection by Delta or BA.1. In doing so, we were able to quantify the impact of antigenic
162 imprinting on *de novo* responses to drifted epitopes.
163

164 **Results:**

165 From our voluntary on-campus testing program at the University of Arizona, we
166 recruited 37 participants who had tested positive for SARS-CoV-2 infections between
167 July 1, 2021 and December 1, 2021 despite completion of the primary vaccine series of
168 monovalent BNT162b2 or mRNA-1273 prior to infection (described in detail in Methods
169 section). We also recruited 12 individuals who tested positive during this period but had
170 not received any COVID-19 vaccines. Symptoms reported by participants following
171 infections were similar between primary and post-vaccination infections; none required
172 hospitalization. A slightly larger portion of post-vaccination infections were
173 asymptomatic relative to primary infections (**Figure S1A**), and in general, the duration of
174 symptoms was significantly shorter in this group relative to those who were
175 unvaccinated at the time of infection (**Figure S1B**). All recruited individuals who tested
176 positive by RT-qPCR and had sufficient sequence coverage to assign a lineage had
177 sequences confirmed to be Delta (**Figure S2A**). During this period, the Delta variant
178 represented 100% of PCR+ samples on campus that could be assigned a PANGO-
179 lineage[87], as determined through viral sequencing of all remnant samples below a Ct
180 value of 35 (**Figure S2B)**. We also selected 71 serum samples as part of our statewide
181 antibody testing initiative[88] from vaccinated participants who had no self-reported prior
182 SARS-CoV-2 infections. This cohort was chosen based on matching for age, sex, and
183 time post-vaccination with our post-vaccination infection group. Characteristics of the
184 cohorts are listed in **Table 1**.

185 Participants provided blood samples at an average of 75 days (IQR for primary
186 and post-vaccination infections = 45.8 days, 97.3 days; **Table 1**) after testing positive for

187 SARS-CoV-2 infections and at an average of nine months (IQR for vaccinated only and
188 post-vaccination infections = 56 days, 317 days; **Table 1**) after their last vaccine dose.
189 Using plasma from these samples, we first performed live virus neutralization assays on
190 both an early-pandemic virus representative, (WA-1, from January 2020) or on the
191 antigenically drifted Delta variant. Against both WA-1 and Delta, post-vaccination Delta
192 infections led to significantly higher titers of neutralizing antibodies than both primary
193 infections and vaccinated only controls (**Figure 1A**), indicating a robust recall response.
194 Elevated neutralizing antibody titers in post-vaccination Delta infections could
195 arise from both memory B cell responses to conserved neutralizing epitopes and
196 primary responses against new variant-specific epitopes. To begin to determine the
197 relative specificities of antibodies following Delta infections, we performed ELISAs to
198 measure the magnitude of the antibody response against Wuhan/Hu1/2019 (hereafter
199 WuHu1) and Delta Spike antigens. WuHu1 was sampled in December 2019 and is the
200 SARS-CoV-2 reference sequence; its Spike amino acid sequence is identical to that of
201 WA-1. We first measured antibodies that bound the receptor binding domain (RBD), as
202 most neutralizing antibodies target this region[89,90]. Post-vaccination Delta infections led
203 to elevated RBD-binding antibody titers, both against WuHu1 and Delta, relative to
204 vaccination only and primary Delta infection controls (**Figure 1B**), again confirming a
205 robust recall response. As expected, vaccination-only controls showed slightly elevated
206 titers of WuHu1 RBD-binding antibodies relative to Delta RBD antibodies (**Figure 1B,**
207 **right panel**). Reciprocally, primary Delta infections led to a skewing towards Delta
208 RBD-binding antibodies (**Figure 1B, right panel**). Post-vaccination-Delta infections led
209 to an even ratio of WuHu1:Delta RBD-binding antibodies (**Figure 1B, right panel**),

210 similar to prior studies[91]. Aside from the RBD, neutralizing antibodies can also bind
211 other regions of the S1 domain of Spike[92–94]. As with RBD, post-vaccination Delta
212 infections led to an even ratio of antibodies that bound WuHu1 and Delta S1 relative to
213 vaccination alone or primary Delta infections (**Figure S3**).

214 To more directly assess antibody specificities with single cell resolution in post-
215 vaccination Delta infections, memory B cells using WuHu1 S1 and Delta S1 antigen
216 tetramers were quantified by flow cytometry. We focused our analysis on the isotype-
217 switched CD27+ subset (**Figure 2A and Figure S4**), since few Spike-specific cells are
218 observed in other memory B cell subsets[95]. Memory B cells that bound Delta S1 only
219 were observed in both primary infections and in post-vaccination Delta infections,
220 suggesting that in both cases, *de novo* responses aimed at variant-unique epitopes
221 were mounted (**Figure 2A-B**). However, the proportions of these cells in PBMCs were
222 slightly reduced in post-vaccination Delta infections relative to primary Delta infections
223 (**Figure 2B**). Reciprocally, cross-reactive memory B cells that bound both WuHu1 S1
224 and Delta S1 were elevated in post-vaccination Delta infections relative to primary Delta
225 infections (**Figure 2B**), consistent with a robust recall response and antigenic imprinting,
226 though for a subset of individuals this appears to be more modest. In both primary and
227 post-vaccination Delta infections, memory B cells that bound Delta S1 uniquely were
228 rare relative to cross-reactive cells that bound both WuHu1 and Delta S1 (**Figures 2A-**
229 **B**). Although these data suggest that pre-existing immunity limits new primary
230 responses, cross-reactive and Delta-specific memory B cells were positively correlated
231 in post-vaccination Delta infections (**Figure 2C**), arguing against a mechanism of
232 competitive inhibition between these two cellular compartments.

233 The RBD of Delta contains two non-synonymous point mutations that deviate
234 from the vaccine sequence: T478K and L452R. The L452R mutation in particular leads
235 to neutralizing antibody escape[90,96–98]. To estimate the epitope preferences of serum
236 antibodies further, we produced a Delta RBD protein in which R452 was reverted to
237 L452. Vaccination led to a response that was skewed toward the L452-containing RBD
238 (**Figure 3A,** compare to **Figure 1B, middle panel**), confirming the strong antibody bias
239 and immunodominance of this epitope reported previously[99]. Yet reciprocal skewing to
240 R452-containing RBD was not observed in primary Delta infections, suggesting that a
241 new immunogenic epitope is not created by this mutation (**Figure 3A**). Post-vaccination
242 Delta infections led to a relatively even ratio of antibodies that bound Delta-L452 to
243 those that reacted to Delta-R452 **(Figure 3A**), perhaps due to boosted levels of
244 antibodies that bound other conserved sites on RBD and the T478K epitope. We also
245 produced chimeric WuHu1 S1 proteins in which the Delta N-terminal domain (NTD)
246 supersite mutations (T19R, G142D, E156-, F157-, R158G) were introduced onto a
247 WuHu1 background[92–94]. Vaccination only controls showed a relatively even distribution
248 of antibodies that bound WuHu1 S1 and Delta NTD-WuHu1 S1 (**Figure 3B** compare to
249 **Figure S3, left panel**). Primary Delta infections, however, were subtly but significantly
250 skewed towards the Delta NTD (**Figure 3B**). Together, these data demonstrate a
251 shifting of immunodominance profiles, even in the absence of prior SARS-CoV-2
252 immunity.
253 To more precisely measure clonal shifts in antibody specificities and
254 immunodominance than can be achieved by serological assays, we performed LIBRA-
255 seq using PBMC samples from primary and post-vaccination Delta infections[100].

256 Streptavidin-phycoerythrin (PE) tetramers were constructed using WuHu1 S1, Delta S1,
257 Delta RBD, Delta RBD-L452, and Delta NTD-WuHu1-S1, as described in **Figures 1, 3**
258 and **S3**, each carrying unique oligonucleotide barcodes. PE-binding memory cells were
259 then enriched and subjected to scRNA/V(D)J-seq. Consistent with our serological data
260 (**Figure 3A-B**), we observed few memory B cells that bound Delta RBD- and NTD-
261 specific epitopes (**Figure 3C**) in primary Delta infections and post-vaccination Delta
262 infections (**Figure S5A**). A clear preference for Delta-unique epitopes in the NTD
263 relative to the RBD was observed within individuals that had experienced a primary
264 Delta infection (**Figure 3D**). Within each group, we did not observe any clear differences
265 in epitope-dependence of somatic mutation frequencies in memory B cells (**Figure**
266 **S5B**). We did, however, observe a greater frequency of somatic mutations in Spike-
267 specific memory B cells in the post-vaccination Delta infection cohort relative to primary
268 Delta infections (**Figure S5C**). Together, these data suggest a marked shift in antibody
269 specificities in primary Delta variant infections relative to WuHu1 Spike. This explains in
270 part why responses to at least some drifted epitopes are not observed, irrespective of
271 prior vaccination.

272 During the course of this work, the heavily mutated Omicron (BA.1) variant
273 rapidly overtook Delta and swept to global dominance. To define post-vaccination BA.1
274 responses, we recruited individuals from our voluntary on-campus testing program who
275 had tested positive for SARS-CoV-2 between January 1 and March 31, 2022, with the
276 expectation that primary responses would be robust against this more antigenically
277 distant variant[101]. All individuals for this study who tested positive by PCR had
278 sequences confirmed to be BA.1 (**Figure S2A**)**.** Individuals with a SARS-CoV-2

279 infection caused by a Delta variant or other Omicron sublineages were excluded from
280 the study. Viral genome sequencing of all remnant PCR+ samples on campus during
281 this period below a Ct value of 35 demonstrated that 93.7% of samples that could be
282 assigned a PANGO-lineage[87] were caused by the BA.1 sublineage of Omicron (**Figure**
283 **S2B**). To obtain controls for this cohort, some of whom had received 3 doses of mRNA
284 vaccines, we also recruited a new group of vaccinated individuals who had never tested
285 positive in our voluntary university testing system and reported no known prior SARS-
286 CoV-2 infections. After testing plasma for nucleocapsid antibodies as a marker of prior
287 infection, samples from 5 individuals with titers well above the mean values seen in
288 verified infections were excluded from further consideration (**Figure S6**). Relative to
289 both primary and post-vaccination Delta infections, post-vaccination BA.1 infections
290 generally led to fewer symptoms such as wet cough (**Figure S1A**) and shorter duration
291 of symptoms (**Figure S1B**).

292 We were unable to recruit any unvaccinated individuals on campus who had
293 experienced BA.1 infections. However, we were able to obtain serum and, for a subset,
294 PBMC samples from a separate study from the Centers for Disease Control and
295 Prevention HEROES and RECOVER projects[85], in which 53 individuals met these
296 criteria (**Table 1**). Neutralizing antibody titers were skewed towards WA-1 in individuals
297 who had been vaccinated but not infected (**Figure 4A**). Post-vaccination BA.1 infections
298 led to significantly higher neutralizing antibody titers against BA.1 compared to both
299 vaccinated controls who had not been infected and primary infections (**Figure 4A**),
300 consistent with a memory B cell recall response.

301 We next examined binding antibody titers against WuHu1 or BA.1 RBD. Post-
302 vaccination BA.1 infections led to increased levels of RBD-binding antibodies, both for
303 WuHu1 and BA.1, relative to the vaccinated only control cohort and primary BA.1
304 infections (**Figure 4B, left and middle panels**). Vaccination alone led to greater RBD
305 titers against BA.1 than did primary BA.1 infections, despite the many mismatches in
306 sequence (**Figure 4B, middle panel**). As expected, antibodies from vaccinated only
307 individuals were skewed towards WuHu1 relative to BA.1 RBD (**Figure 4B, right**
308 **panel**). Of the few antibodies induced by primary BA.1 infections, we observed a
309 skewing of specificities towards BA.1 RBD (**Figure 4B, right panel**). Ratios of WuHu1
310 and BA.1 RBD-binding antibodies in post-vaccination BA.1 infections more closely
311 resembled vaccinated controls than primary BA.1 infections (**Figure 4B, right panel**).

312 To further evaluate the specificities of antibody responses in post-vaccination
313 BA.1 infections, we again used antigen tetramers to identify RBD-specific memory B
314 cells (**Figures S7 and 5A**). As expected, primary BA.1 infections generated a lower
315 frequency of WuHu1 RBD-specific memory B cells compared to vaccinated controls
316 (**Figure 5B, left panel**). Unexpectedly, BA.1-specific RBD memory B cells were not
317 consistently detectable above background in any experimental group, even primary
318 BA.1 infections (**Figure 5B, middle panel**). These data seem to differ from the modest
319 skewing of the serological response seen above in primary BA.1 infections (**Figure 4B,**
320 **right panel**), but can potentially be explained by low overall responses and prior studies
321 that observed only partial overlap between memory B and antibody-secreting plasma
322 cell specificities and repertoires[43,102,103]. Instead, most RBD-specific memory B cells
323 from all cohorts were cross-reactive against WuHu1 and BA.1 RBD (**Figure 5A, 5B,**

324 **right panel**). Primary BA.1 infections produced numerically fewer cross-reactive RBD
325 memory B cells than did post-vaccination BA.1 infections (**Figure 5B, right panel**).

326 Given that the overall antibody and memory B cell response to BA.1 RBD was
327 quite modest (**Figures 4B, 5A-B**), we employed tetramers of full-length Spike trimers of
328 WuHu1 and BA.1 Spike to capture a greater breadth of memory B cell specificities than
329 could be observed with RBD tetramers (**Figures 5C**). WuHu1-specific memory B cells
330 were observed in vaccinated controls and post-vaccination BA.1 infections, but not after
331 primary BA.1 infections (**Figures 5D, left panel**). We again failed to consistently
332 observe BA.1-specific memory B cells in any of the groups, including primary BA.1
333 infections, though a subset of post-vaccination BA.1 infections did appear to generate
334 such cells well above background levels (**Figure 5D, middle panel**). As with RBD,
335 cross-reactive Spike-specific memory cells were significantly elevated in post-
336 vaccination BA.1 infections relative to primary BA.1 infections, but not relative to
337 vaccinated only controls (**Figure 5D, right panel**). Cross-reactive memory B cells
338 composed by far the largest portion of SARS-CoV-2 specific responses within all
339 experimental groups (**Figure S8**).

340 For a subset of primary BA.1 and post-vaccination BA.1 cohorts, we obtained
341 samples which enabled us to quantify WuHu1, BA.1, and cross-reactive Spike- and
342 RBD- specific memory B cell frequencies before and after BA.1 infection. Irrespective of
343 vaccination status, memory B cells that were either WuHu1- or BA.1-RBD-specific
344 increased in frequency for only a subset of individuals after BA.1 infection (**Figure 6A,**
345 **left and middle panels**). However, cross-reactive RBD memory B cells consistently
346 and significantly increased after both primary and post-vaccination BA.1 infections

347 (**Figure 6A, right panel**). The frequency of cross-reactive Spike memory B cells also
348 significantly increased after primary BA.1 infections (**Figures 6B, right panel**).

349 To infer potential mechanisms of antigenic imprinting from these samples, we
350 first correlated pre-infection cross-reactive Spike-specific memory B cells and post-
351 infection BA.1 Spike-specific memory B cells. A negative correlation could indicate
352 detrimental imprinting, whereby pre-existing memory B cells outcompete naïve B cells
353 and inhibit the generation of variant-specific responses. Instead, we observed a slight
354 positive but non-statistically significant correlation between pre-infection cross-reactive
355 Spike-specific memory B cells and post-infection BA.1 Spike-specific memory B cells
356 (**Figure 7A**). Similarly, we observed a non-significant positive correlation between post-
357 infection cross-reactive Spike-specific memory B cells and post-infection BA.1 Spike-
358 specific memory B cells (**Figure 7B**).

359 Given that these data do not support a mechanism of competitive inhibition of
360 naïve B cells by cross-reactive memory B cells, we explored other mechanisms by
361 which *de novo* responses to drifted epitopes are indirectly suppressed, such as
362 accelerated viral clearance by neutralizing antibodies and/or T cells. We found a
363 negative, but non-statistically significant correlation of *de novo* responses with pre-
364 infection BA.1 neutralizing antibody titers (**Figure 7C**). Similarly, we observed a small
365 and non-significant negative correlation with pre-infection BA.1 Spike-specific T cell
366 numbers and post-infection BA.1 Spike memory B cells (**Figure 7D**). The small sample
367 sizes and variable times of blood sampling prior to infection preclude us from making
368 definitive conclusions about mechanisms driving antigenic imprinting. Nonetheless, the
369 data suggest that neutralizing antibody and/or memory T cell-mediated viral clearance

370 may indirectly underlie suppression of responses to drifted epitopes. This overall impact
371 is quite small relative to the marked changes in antibody immunodominance observed
372 in even primary BA.1 variant infections, irrespective of prior immunity.

373 **Discussion:**

374 Antigenic imprinting is neither inherently beneficial nor detrimental; rather the
375 impact of prior immunity is context-dependent[45]. For example, pre-existing serum
376 antibodies can improve and focus *de novo* responses upon reinfection to only mutated
377 novel epitopes through epitope masking[104–106]. Similarly, *de novo* responses to drifted
378 epitopes can be improved by pre-existing CD4+ memory T cells in what is classically
379 known as the hapten-carrier effect[107]. Alternatively, high affinity memory B cells can
380 competitively inhibit naïve B cells by consuming limited amounts of antigen and T cell
381 help, leading to a suppression of *de novo* antibody responses[108]. If these memory B
382 cells target non-protective epitopes, this could in theory leave one worse off than if there
383 were no prior immunity whatsoever[44,109]. Finally, pre-existing immunity could indirectly
384 suppress new antibody responses to drifted epitopes simply by clearing away virus and
385 antigen before naïve B cells can robustly participate.

386 Though neutralizing antibody titers were robust following post-vaccination
387 infections, our results demonstrated a small negative impact of prior immunity on *de*
388 *novo* responses to drifted epitopes. Yet we found no evidence to support a mechanism
389 of competitive inhibition by cross-reactive memory B cells. Though not definitive, our
390 data instead hint at a role for pre-infection neutralizing antibodies and memory T cells,
391 suggesting that antigen clearance is the main mechanism by which *de novo* B cell
392 responses are indirectly suppressed by prior immunity. Indeed, pre-existing neutralizing
393 antibodies likely accelerate viral clearance[110,111], and viral and vaccine antigens can
394 potentially also be cleared by T cells or non-neutralizing antibodies via Fc effector
395 functions[112–114]. Animal studies offer an attractive way to further test mechanisms of

396 antigenic imprinting on heterologous vaccine and viral infection responses. For
397 example, genetic tracking studies were used to show robust *de novo* responses to
398 Omicron boosters in mice previously vaccinated against the ancestral strain. Yet this
399 required two booster doses, and a small negative impact of prior immunity was
400 observed in inverse proportion to the antigenic distance between the two
401 immunizations[101]. Similar results have been reported in other mouse studies[115]. These
402 systems can thus potentially be used to manipulate specific immune parameters and
403 measure their contributions to antigenic imprinting in ways that are not possible in
404 human studies, especially since few immunologically naïve adults remain to serve as
405 controls.

406 Immunodominance hierarchies can also determine which epitopes are available
407 to be targeted by antibodies, irrespective of prior immunity. Prior studies, confirmed in
408 our experiments, showed that a large portion of COVID-19 vaccine-induced antibodies
409 are aimed at the L452 class 3 epitope[116]. Yet in the post-vaccination Delta cohort, we
410 observed few antibodies directed at the epitope containing the L452R mutation. Under
411 the assumption that one immunodominant epitope was being mutated to another, one
412 might have concluded that the absence of R452-specific antibodies could be explained
413 by antigenic imprinting. Yet by including a primary infection cohort, we observed that the
414 Delta variant intrinsically did not elicit detectable antibody responses against the R452
415 epitope, even with no prior SARS-CoV-2 exposures, consistent with an independent
416 study[52]. We can instead conclude that Delta shifts antibody immunodominance
417 hierarchies to instead focus more on epitopes located in the NTD. These types of shifts
418 in immunodominance preempt any considerations of the impact of antigenic imprinting.

419 The basis and mechanisms of these shifts for SARS-CoV-2 clearly needs more
420 investigation to determine whether and how best to overcome them.

421 This study spanned a period from the Delta wave through the more antigenically
422 distinct BA.1 Omicron wave. A central expectation of antigenic imprinting is that the
423 extent to which prior immunity interferes with *de novo* responses should decrease as
424 antigenic distance increases[101]. We used the Delta and BA.1 variants to test this
425 expectation in SARS-CoV-2 and to understand the impacts of antigenic distance on
426 antigenic imprinting. Despite our prediction, we observe even less of a variant specific
427 response in post-vaccination BA.1 infections compared to post-vaccination Delta
428 infections. Much of this can be explained by shifts in immunodominance in which even
429 primary BA.1 infections elicited few memory B cell responses to drifted epitopes. Yet
430 longitudinal sampling during BA.1 infections has also shown that viral titers do not reach
431 the peak levels observed in Delta infections[117], suggesting that immune responses to
432 drifted epitopes occur in proportion to need and antigen availability.

Disclosures: The findings and conclusions in this report are those of the authors and do not necessarily represent the official position of the Centers for Disease Control and Prevention.

Acknowledgements: This work was supported by NIH grants R01AI099108 and R01AI129945 (D.B.) and a research grant from the Arizona Board of Regents (M.W. and D.B). This project has been funded in part with Federal funds from the National Institute of Allergy and Infectious Diseases, National Institutes of Health, Department of Health and Human Services, under Contract No. 75N93021C00015 (M.W.) The HEROES-RECOVER cohort is supported by the National Center for Immunization and Respiratory Diseases and the Centers for Disease Control and Prevention (contracts 75D30120R68013 to Marshfield Clinic Research Institute, 75D30120C08379 to the University of Arizona, and 75D30120C08150 to Abt Associates).

Declaration of Interests: Sana Biotechnology has licensed intellectual property of D.B. and Washington University in St. Louis. Gilead Sciences has licensed intellectual property of D.B. and Stanford University. Clade Therapeutics has licensed intellectual property of D.B. and University of Arizona. D.B. is a co-founder of Clade Therapeutics. D.B. served on an advisory panel for GlaxoSmithKline. B.J.L. has a financial interest in Cofactor Genomics, Inc. and Iron Horse Dx. Geneticure Inc. has licensed intellectual property of R.S. and R.S is a co-founder of Geneticure Inc. M.W. has received consulting fees from GLG on SARS-CoV-2 and the COVID-19 pandemic.

456 **Methods:**

457

458 ***Participant selection***

459 All human studies conducted at The University of Arizona were approved by the
460 Institutional Review Board for the Human Subjects Protection Program[†]. Individuals who
461 had participated in the voluntary on-campus saline gargle testing program and had
462 either never tested positive or had tested positive during the Delta or BA.1 waves were
463 contacted by email by the program administrators (not the authors on this study) about
464 willingness to participate in this research study. Participants were provided a link to an
465 eligibility questionnaire and, once eligibility (no immunosuppressive therapy in the last 5
466 years and HIV negative) was confirmed, additional demographic questions and a link to
467 schedule an appointment for blood draws. Written consent was obtained through an
468 electronic form. All blood draws were performed at the Clinical and Translational
469 Sciences Center at The University of Arizona. Additional primary and post-vaccination
470 BA.1 infection samples were acquired from the CDC HEROES-RECOVERS[††] cohort[85].
471 This study was reviewed by CDC and approved by the institutional review boards at
472 participating sites or under a reliance agreement with Abt Associates institutional review
473 board and was conducted consistent with applicable federal law and CDC policy under
474 45 C.F.R. part 46, 21 C.F.R. part 56, 42 U.S.C. Sect. 241(d), 5 U.S.C. Sect. 552a, 44
475 U.S.C. Sect. 3501 et seq. Methods for the HEROES-RECOVER Cohorts have
476 been published previously[85,86]. In summary, cohorts consisted of health care
477 personnel, first responders, and other essential and frontline workers in eight
478 U.S. locations across six states. Participants collected weekly nasal swabs which

479 were tested for SARS-CoV-2 viral material by RT-qPCR and additional swabs
480 were collected and screened upon the onset of any COVID-19–like illness
481 symptoms. In addition, blood draws were collected at enrollment, then
482 approximately every 3 months and after immune modifying events such as
483 vaccination or infection. Vaccination was documented by self-report and verified
484 by vaccine cards or electronic medical records or state immunization registries.
485 HEROES-RECOVER participants were selected based on testing positive for SARS-
486 CoV-2 during Delta or BA.1 waves and having completed a blood draw after infection.
487

488 ***Saline Gargle PCR testing for SARS-CoV-2***

489 As part of Test All, Test Smart, the University of Arizona's voluntary campus-wide
490 testing program, University staff, faculty and students had access to SARS-CoV-2 rRT-
491 PCR tests from August 2020 – July 2023. At testing and collection sites throughout
492 campus, individuals were given 5 mL of 0.9 % sterile saline (AddiPak 5 mL sterile saline
493 single use tubes, Teleflex, LLC) and guided to complete three rounds of a 5-second
494 swish followed by 10 seconds of gargling (adapted from Goldfarb et al.[118]). Samples
495 were deposited into collection tubes and then screened for SARS-CoV-2 by rRT-PCR.
496

497 ***PBMC and plasma preparation***

498 Twenty milliliters of blood was collected by venipuncture in heparinized Vacutainer
499 tubes (BD). For PBMCs, 15ml of Ficoll-Paque PLUS (Thermo Fisher Scientific) was
500 added to 50-ml Leucosep tubes (Greiner) and spun for 1min at 1,000g to transfer the
501 density gradient below the filter. Twenty milliliters of blood from the heparinized tubes

502 was then poured into the top of the Leucosep tube and spun at 1,000g for 10min at
503 room temperature with the brake off. The top plasma layer was carefully collected and
504 frozen at −20 °C, and the remaining supernatant containing PBMCs above the filter was
505 poured into a new 50-ml conical tube containing 10mL of PBS and spun at 250g for
506 10min. Cell pellets were resuspended in RPMI media containing 10% FCS and counted
507 on a Vi-Cell XR (Beckman Coulter). Cells were diluted to a concentration of 2×10^7
508 cells per mL in RPMI media containing 10% FCS. An equal volume of 80% FCS + 20%
509 dimethyl sulfoxide was added dropwise and inverted once to mix. Suspensions were
510 distributed at 1ml per cryovial and frozen overnight at −80 °C in Mr. Frosty freezing
511 chambers (Nalgene). Vials were then transferred to storage in liquid nitrogen.
512
513
514 ***ELISA and quantification of antibody titers***
515 Serological assays were performed as previously described[88]. WuHu1 RBD (cat. no.
516 SPD-C52H3), WuHu1 S1subdomain of the SARS-CoV-2 S glycoprotein (cat. no. S1N-
517 C52H3), WuHu1 Spike (cat. no. SPN-C52H9), Delta RBD (cat. no. SPD-C52Hh), Delta
518 S1 subdomain (cat. no. S1N-C52Hu), Omicron (BA.1) RBD (cat. no. SPD-C522e),
519 Omicron (BA.1) Spike (cat. no. SPN-C52Hz) and Nucleocapsid (cat. no. NUN-C5227)
520 were purchased from Acro Biosystems. Chimeric proteins (Delta RBD-L452 and Delta
521 NTD-WuHu1 S1) were custom synthesized by GenScript. To obtain titers and single-
522 dilution OD450 values, antigens were immobilized on high-adsorbency 384-well plates
523 at 5 ng mL^{-1}. Plates were blocked with 1% non-fat dehydrated milk extract (Santa Cruz
524 Biotechnology, sc-2325) in sterile PBS (Thermo Fisher Scientific HyClone PBS,

525 SH2035) for 1 h, washed with PBS containing 0.05% Tween-20 and overlaid for 60 min
526 with either a single 1:60 dilution or five serial 1:3 dilutions beginning at a 1:60 dilution of
527 serum. Plates were then washed and incubated for 1 h in 1% PBS and milk containing
528 anti-human Pan-Ig HRP-conjugated antibody (Jackson ImmunoResearch, 109-035-064)
529 at a concentration of 1:2,000 for 1 h. Plates were washed with PBS-Tween solution
530 followed by PBS wash. To develop, plates were incubated in tetramethylbenzidine
531 (Fisher Scientific) before quenching with 2 N H_2SO_4. Plates were read for 450-nm
532 absorbance on CLARIOstar Plus from BMG Labtech. All samples were also read at
533 630 nm to detect any incomplete quenching. Any samples above background 630-nm
534 values were re-run. Area under the curve (AUC) values were calculated in GraphPad
535 Prism (v9).
536
537
538 ***Virus neutralization assays***
539 All live virus assays were performed at Biosafety Level 3 and were approved by the
540 University of Arizona Institutional Biosafety Committee. SARS-CoV-2, isolate USA-
541 WA1/2020, was deposited by Dr Natalie J. Thornburg at the Centers for Disease
542 Control and Prevention and obtained from the World Reference Center for Emerging
543 Viruses and Arboviruses. Stocks of WA1/2020 SARS-CoV-2 were generated as a single
544 passage from received stock vial on mycoplasma-negative Vero cells (ATCC CCL-81).
545 B.1.617.2 (Delta) was received from WRCEVA, strain designation GNL-1205. B.1.1.529
546 (Omicron) originated from a nasopharyngeal swab collected at the University of Arizona.
547 It was passaged once on Calu-3 cells and then once on Vero cells to generate a master

548 stock. Viral PANGO-lineage, BA.1.1[87], was confirmed by Illumina sequencing
549 (EPI_ISL_17886211) of the master stock.
550 Supernatant and cell lysate were combined, subjected to a single freeze–thaw
551 and then centrifuged at 1,800g for 10min to remove cell debris. For PRNTs for SARS-
552 CoV-2, Vero cells (ATCC, CCL-81) were plated in 96-well tissue culture plates and
553 grown overnight. Vero cells were confirmed by PCR to be free of mycoplasma using the
554 Universal Mycoplasma Detection Kit (ATCC). Serial dilutions of serum samples were
555 performed in duplicate and incubated with 100 plaque-forming units of SARS-CoV-2 for
556 1h at 37 °C. Plasma/serum dilutions plus virus were transferred to the cell plates and
557 incubated for 2h at 37 °C in 5% CO2 and then overlaid with 1% methylcellulose. After
558 72h, plates were fixed with 10% neutral buffered formalin for 30min and stained with 1%
559 crystal violet. Plaques were imaged using an ImmunoSpot Versa plate reader. The most
560 dilute serum concentration that led to ten or fewer plaques was designated as the
561 PRNT90 titer. Input PFU for each experiment was confirmed by plaque assay.
562
563 ***Flow cytometry***
564 One milliliter of pre-warmed FBS was added to a frozen cryovial of 10^7 PBMCs, which
565 was rapidly thawed in a 37℃ water bath. Samples were poured into 15 mL conical tubes
566 containing 5 mL of pre-warmed RPMI with 5% FBS and 1% anti/anti. Tubes were spun
567 at 250g for 5 min at room temperature.
568 **Delta**
569 Supernatants were removed and cell pellets were resuspended in 200 µL of staining
570 buffer containing 1 µL each of anti-CD38-APC (BioLegend, clone HIT2), anti-CD13-PE-

571 Cy7 (BioLegend, clone WM15), anti-CD21-PE-Dazzle (BioLegend, clone Bu32), anti-
572 CD19-APC-efluor-780 (Invitrogen, clone HIB19), anti-IgD-PerCP-Cy5.5 (Biolegend,
573 clone IA6-2), anti-IgM-FITC (Biolegend, clone MHM-88), anti-CD27-BV510 (Biolegend,
574 clone M-T271), anti-CD11c-Alexa700 (BioLegend, clone Bu15). Staining buffer also
575 contained Delta-S1-PE and S1-BV421 tetramers.

576 **BA.1**

577 Supernatants were removed and cell pellets were resuspended in 200 µL of staining
578 buffer containing 1 µL each of anti-CD38-BV421 (BioLegend, clone HB-7), anti-CD13-
579 PE-Dazzle 594 (BioLegend, clone WM15), anti-CD21-PerCP Cy 5.5 (BioLegend, clone
580 Bu32), anti-CD19-APC-efluor-780 (Invitrogen, clone HIB19), anti-IgD-BV510
581 (Biolegend, clone 11-26c.2a), anti-IgM-FITC (Biolegend, clone MHM-88), anti-CD27-PE
582 Cy 7 (Biolegend, clone M-T271), anti-CD11c-Alexa700 (BioLegend, clone Bu15). Cells
583 were stained with live-dead marker, Zombie Yellow (BioLegend) according to
584 manufacturer's recommendations. Staining buffer also contained BA.1-Spike-PE and
585 Spike-Alexa Fluor 647 tetramers.

586

587 Antibodies were validated by the manufacturer on human PBMCs. Tetramer reagents
588 were assembled by mixing 100µg ml^{-1} of C-terminal AviTagged S1, Delta S1, WuHu1
589 Spike, or BA.1 Spike (ACROBiosystems) with 100µg ml^{-1} of streptavidin-PE(BioLegend),
590 streptavidin-BV421 (BioLegend), or streptavidin-Alexa Fluor 647 (BioLegend),
591 respectively, at a 6:1 molar ratio for S1 or 4:1 molar ratio for Spike, in which ⅕ of the
592 final volume of streptavidin was added every 10 min. S1 and Spike tetramers were
593 validated by staining Lenti-X 293T cells(Takara Bio) as a negative control or 293T-

594 hACE2-expressing cells (BEI Resources, NR-52511) as a positive control. Lenti-X 293T
595 cells were confirmed to be free of mycoplasma; 293T-hACE2 cells were maintained in
596 media containing 1% pen/strep to minimize chances of contamination. PBMC samples
597 were stained for at least 20 minutes, washed and filtered through 70-µm nylon mesh.
598 Data were analyzed on either a BD LSR2 (tetramer validation only), a Fortessa
599 cytometer (Delta), or BD Cytek Aurora (BA.1). Data were analyzed using FlowJo
600 software.
601
602 ***Flow cytometry and Fluorescence Activated Cell Sorting***
603 One milliliter of pre-warmed FBS was added to a frozen cryovial of PBMCs and thawed
604 by pipetting. Samples were added to 15 mL conical tubes containing 10 mL of pre-
605 warmed RPMI with 20% FBS and 1% anti/anti. Tubes were spun at 1200 RPM for 5
606 minutes at room temperature. Supernatants were removed and cell pellets were
607 resuspended in 200 µL of staining buffer contained 1 µL each of anti-CD19-
608 BV421(Biolegend, clone HIB19), anti-CD27-FITC(Biolegend, clone O323), anti-CD13-
609 PE-Cy-7(Biolegend, clone WM15), anti-IgD-APC-Cy-7(Biolegend, clone IA6-2). Staining
610 buffer also contained either 5 or 2 LIBRA-Seq tetramers: S1-PE(Biolegend, TotalSeq-
611 C0951_PE), Delta S1-PE(Biolegend, TotalSeq-C0952_PE), Delta NTD/S1-
612 PE(Biolegend, TotalSeq-C0953_PE), Delta RBD/L452(Biolegend, TotalSeq-
613 C0954_PE), and Delta RBD-PE(Biolegend, TotalSeq-C0955_PE). Biotinylated tetramer
614 reagents were assembled by mixing 100µg ml^{-1} of C-terminal AviTagged S1
615 (ACROBiosystems), Delta S1 (ACROBiosystems), Delta NTD/S1 (GenScript), Delta
616 RBD/L452 (Genscript), or Delta RBD (ACROBiosystems) with 100µg ml^{-1} of

617 streptavidin-TotalSeq-C-PE (BioLegend) at a 6:1 molar ratio in which ⅕ of the final
618 volume of streptavadin was added every 10 min. Tetramers were validated by staining
619 Lenti-X 293T cells(Takara Bio) as a negative control or 293T-hACE2-expressing cells
620 (BEI Resources, NR-52511) as a positive control. Lenti-X 293T cells were confirmed to
621 be free of mycoplasma; 293T-hACE2 cells were maintained in media containing 1%
622 pen/strep to minimize chances of contamination. Additionally, TotalSeq-C anti-human
623 Hashtag antibodies (Biolegend, TotalSeq™-C0251-10) were added to individual
624 samples and pooled after staining and washing. PBMCs were stained in the dark for 30
625 minutes at 4˚C, washed, pooled and filtered through a 35 µm strainer (Fisher Scientific).
626 SARS-CoV-2 specific memory B cells (CD19+IgD-IgM-CD27+) as well as non-antigen
627 specific memory B cells were sorted using a FACSAria II.
628
629 ***Single-cell RNA sequencing and analysis***
630 Cells were prepared and processed according to the 10X Genomics Single Cell 5' Dual
631 Index protocol with Feature Barcoding Technology for Cell Surface Protein and Immune
632 Receptor Mapping kit (10X Genomics). Reads were processed and aligned using the
633 10X CellRanger multi pipeline to GRCh38 gex and vdj reference genomes (10X
634 Genomics). Each sample feature barcode matrix was loaded into R and analyzed
635 utilizing the Seurat package for gene expression, vdj and antibody capture analysis[119].
636 Cell processing was conducted as previously described[100]. Data are available at NCBI
637 GEO accession number GSE242775.
638
639 ***ELISpot Assay***

640 Cryopreserved PBMC (5 × 10^6/sample) were thawed in prewarmed RPMI-1640 media
641 supplemented with L-glutamine + 10% FCS and 300ug DNAse. Thawed PBMCs were
642 rested overnight at 37 °C in X-VIVO™-15 Medium (Lonza) supplemented with 5%
643 human-AB serum. Cells were stimulated with ~1 nmol of peptide pool corresponding to
644 spike of Omicron (B.1.1.529) variant (16-mer peptide pools, overlapping by 10 amino
645 acids (21st century Biochemicals Inc.) on pre-coated human IFN-γ ELISpot plates
646 (Mabtech, Inc.) and developed after 18 hours according to manufacturer instructions.
647 Spots were imaged and counted using Iris FLUOROspot reader (Mabtech).
648
649 ***Statistical methods***
650 All analyses are listed in the figure legends and were performed in GraphPad Prism 9
651 and/or the R programming language (v4.0.5).
652
653 **Footnotes**
654 † See 45 C.F.R. part 46; 21 C.F.R. part 56
655 †† This study was reviewed by CDC and approved by the institutional review boards at
656 participating sites or under a reliance agreement with Abt Associates institutional review
657 board and was conducted consistent with applicable federal law and CDC policy under
658 45 C.F.R. part 46, 21 C.F.R. part 56, 42 U.S.C. Sect. 241(d), 5 U.S.C. Sect. 552a, 44
659 U.S.C. Sect. 3501 et seq.
660
661
662

663 ***References***

664 1. Novel 2019 coronavirus genome (2020). Virological. https://virological.org/t/novel-
665 2019-coronavirus-genome/319.

666 2. Baden, L.R., El Sahly, H.M., Essink, B., Kotloff, K., Frey, S., Novak, R., Diemert, D.,
667 Spector, S.A., Rouphael, N., Creech, C.B., et al. (2021). Efficacy and safety of the
668 mRNA-1273 SARS-CoV-2 vaccine. N. Engl. J. Med. *384*, 403–416.
669 10.1056/NEJMoa2035389.

670 3. Polack, F.P., Thomas, S.J., Kitchin, N., Absalon, J., Gurtman, A., Lockhart, S.,
671 Perez, J.L., Pérez Marc, G., Moreira, E.D., Zerbini, C., et al. (2020). Safety and
672 Efficacy of the BNT162b2 mRNA Covid-19 Vaccine. N. Engl. J. Med. *383*, 2603–
673 2615. 10.1056/NEJMoa2034577.

674 4. Sadoff, J., Gray, G., Vandebosch, A., Cárdenas, V., Shukarev, G., Grinsztejn, B.,
675 Goepfert, P.A., Truyers, C., Fennema, H., Spiessens, B., et al. (2021). Safety and
676 efficacy of single-dose Ad26.COV2.S vaccine against Covid-19. N. Engl. J. Med.
677 *384*, 2187–2201. 10.1056/NEJMoa2101544.

678 5. Tanriover, M.D., Doğanay, H.L., Akova, M., Güner, H.R., Azap, A., Akhan, S., Köse,
679 Ş., Erdinç, F.Ş., Akalın, E.H., Tabak, Ö.F., et al. (2021). Efficacy and safety of an
680 inactivated whole-virion SARS-CoV-2 vaccine (CoronaVac): interim results of a
681 double-blind, randomised, placebo-controlled, phase 3 trial in Turkey. Lancet *398*,
682 213–222. 10.1016/S0140-6736(21)01429-X.

683 6. Heath, P.T., Galiza, E.P., Baxter, D.N., Boffito, M., Browne, D., Burns, F.,
684 Chadwick, D.R., Clark, R., Cosgrove, C., Galloway, J., et al. (2021). Safety and
685 efficacy of NVX-CoV2373 covid-19 vaccine. N. Engl. J. Med. *385*, 1172–1183.
686 10.1056/NEJMoa2107659.

687 7. Voysey, M., Clemens, S.A.C., Madhi, S.A., Weckx, L.Y., Folegatti, P.M., Aley, P.K.,
688 Angus, B., Baillie, V.L., Barnabas, S.L., Bhorat, Q.E., et al. (2021). Safety and
689 efficacy of the ChAdOx1 nCoV-19 vaccine (AZD1222) against SARS-CoV-2: an
690 interim analysis of four randomised controlled trials in Brazil, South Africa, and the
691 UK. Lancet *397*, 99–111. 10.1016/S0140-6736(20)32661-1.

692 8. Xia, S., Zhang, Y., Wang, Y., Wang, H., Yang, Y., Gao, G.F., Tan, W., Wu, G., Xu,
693 M., Lou, Z., et al. (2021). Safety and immunogenicity of an inactivated SARS-CoV-2
694 vaccine, BBIBP-CorV: a randomised, double-blind, placebo-controlled, phase 1/2
695 trial. Lancet Infect. Dis. *21*, 39–51. 10.1016/S1473-3099(20)30831-8.

696 9. Pouwels, K.B., Pritchard, E., Matthews, P.C., Stoesser, N., Eyre, D.W., Vihta, K.-D.,
697 House, T., Hay, J., Bell, J.I., Newton, J.N., et al. (2021). Effect of Delta variant on
698 viral burden and vaccine effectiveness against new SARS-CoV-2 infections in the
699 UK. Nat. Med. *27*, 2127–2135. 10.1038/s41591-021-01548-7.

700 10. Chen, J., Wang, R., Gilby, N.B., and Wei, G.-W. (2022). Omicron variant
701 (B.1.1.529): Infectivity, vaccine breakthrough, and antibody resistance. J. Chem. Inf.
702 Model. *62*, 412–422. 10.1021/acs.jcim.1c01451.

703 11. Tao, K., Tzou, P.L., Nouhin, J., Gupta, R.K., de Oliveira, T., Kosakovsky Pond, S.L.,
704 Fera, D., and Shafer, R.W. (2021). The biological and clinical significance of
705 emerging SARS-CoV-2 variants. Nat. Rev. Genet., 1–17. 10.1038/s41576-021-
706 00408-x.

707 12. Dejnirattisai, W., Huo, J., Zhou, D., Zahradník, J., Supasa, P., Liu, C., Duyvesteyn,
708 H.M.E., Ginn, H.M., Mentzer, A.J., Tuekprakhon, A., et al. (2022). SARS-CoV-2
709 Omicron-B.1.1.529 leads to widespread escape from neutralizing antibody
710 responses. Cell. 10.1016/j.cell.2021.12.046.

711 13. Gilbert, P.B., Montefiori, D.C., McDermott, A.B., Fong, Y., Benkeser, D., Deng, W.,
712 Zhou, H., Houchens, C.R., Martins, K., Jayashankar, L., et al. (2022). Immune
713 correlates analysis of the mRNA-1273 COVID-19 vaccine efficacy clinical trial.
714 Science *375*, 43–50. 10.1126/science.abm3425.

715 14. Khoury, D.S., Cromer, D., Reynaldi, A., Schlub, T.E., Wheatley, A.K., Juno, J.A.,
716 Subbarao, K., Kent, S.J., Triccas, J.A., and Davenport, M.P. (2021). Neutralizing
717 antibody levels are highly predictive of immune protection from symptomatic SARS-
718 CoV-2 infection. Nat. Med. *27*, 1205–1211. 10.1038/s41591-021-01377-8.

719 15. Rausch, J.W., Capoferri, A.A., Katusiime, M.G., Patro, S.C., and Kearney, M.F.
720 (2020). Low genetic diversity may be an Achilles heel of SARS-CoV-2. Proc. Natl.
721 Acad. Sci. U. S. A. *117*, 24614–24616. 10.1073/pnas.2017726117.

722 16. Volz, E. (2023). Fitness, growth and transmissibility of SARS-CoV-2 genetic
723 variants. Nat. Rev. Genet., 1–11. 10.1038/s41576-023-00610-z.

724 17. Wiegand, T., Nemudryi, A., Nemudraia, A., McVey, A., Little, A., Taylor, D.N., Walk,
725 S.T., and Wiedenheft, B. (2022). The Rise and Fall of SARS-CoV-2 Variants and
726 Ongoing Diversification of Omicron. Viruses *14*, 2009. 10.3390/v14092009.

727 18. Hill, V., Du Plessis, L., Peacock, T.P., Aggarwal, D., Colquhoun, R., Carabelli, A.M.,
728 Ellaby, N., Gallagher, E., Groves, N., Jackson, B., et al. (2022). The origins and
729 molecular evolution of SARS-CoV-2 lineage B.1.1.7 in the UK. Virus Evol. *8*,
730 veac080. 10.1093/ve/veac080.

731 19. Cao, Y., Song, W., Wang, L., Liu, P., Yue, C., Jian, F., Yu, Y., Yisimayi, A., Wang,
732 P., Wang, Y., et al. (2022). Characterization of the enhanced infectivity and
733 antibody evasion of Omicron BA.2.75. Cell Host Microbe *30*, 1527-1539.e5.
734 10.1016/j.chom.2022.09.018.

735 20. Volz, E., Mishra, S., Chand, M., Barrett, J.C., Johnson, R., Geidelberg, L., Hinsley,
736 W.R., Laydon, D.J., Dabrera, G., O'Toole, Á., et al. (2021). Assessing
737 transmissibility of SARS-CoV-2 lineage B.1.1.7 in England. Nature *593*, 266–269.
738 10.1038/s41586-021-03470-x.

739 21. Cherian, S., Potdar, V., Jadhav, S., Yadav, P., Gupta, N., Das, M., Rakshit, P.,
740 Singh, S., Abraham, P., Panda, S., et al. (2021). Convergent evolution of SARS-
741 CoV-2 spike mutations, L452R, E484Q and P681R, in the second wave of COVID-
742 19 in Maharashtra, India. bioRxiv, 2021.04.22.440932. 10.1101/2021.04.22.440932.

743 22. Cheng, Y.-W., Chao, T.-L., Li, C.-L., Wang, S.-H., Kao, H.-C., Tsai, Y.-M., Wang,
744 H.-Y., Hsieh, C.-L., Lin, Y.-Y., Chen, P.-J., et al. (2021). D614G Substitution of

745 SARS-CoV-2 Spike Protein Increases Syncytium Formation and Virus Titer via
746 Enhanced Furin-Mediated Spike Cleavage. MBio, e0058721. 10.1128/mBio.00587-
747 21.

748 23. McCallum, M., Bassi, J., De Marco, A., Chen, A., Walls, A.C., Di Iulio, J., Tortorici,
749 M.A., Navarro, M.-J., Silacci-Fregni, C., Saliba, C., et al. (2021). SARS-CoV-2
750 immune evasion by the B.1.427/B.1.429 variant of concern. Science.
751 10.1126/science.abi7994.

752 24. Imai, M., Halfmann, P.J., Yamayoshi, S., Iwatsuki-Horimoto, K., Chiba, S.,
753 Watanabe, T., Nakajima, N., Ito, M., Kuroda, M., Kiso, M., et al. (2021).
754 Characterization of a new SARS-CoV-2 variant that emerged in Brazil. PNAS.
755 10.1073/pnas.2106535118/-/DCSupplemental.

756 25. Viana, R., Moyo, S., Amoako, D.G., Tegally, H., Scheepers, C., Althaus, C.L.,
757 Anyaneji, U.J., Bester, P.A., Boni, M.F., Chand, M., et al. (2022). Rapid epidemic
758 expansion of the SARS-CoV-2 Omicron variant in southern Africa. Nature *603*,
759 679–686. 10.1038/s41586-022-04411-y.

760 26. Sokal, A., Chappert, P., Barba-Spaeth, G., Roeser, A., Fourati, S., Azzaoui, I.,
761 Vandenberghe, A., Fernandez, I., Meola, A., Bouvier-Alias, M., et al. (2021).
762 Maturation and persistence of the anti-SARS-CoV-2 memory B cell response. Cell
763 *184*, 1201-1213.e14. 10.1016/j.cell.2021.01.050.

764 27. Muecksch, F., Weisblum, Y., Barnes, C.O., Schmidt, F., Schaefer-Babajew, D.,
765 Wang, Z., C Lorenzi, J.C., Flyak, A.I., DeLaitsch, A.T., Huey-Tubman, K.E., et al.

766 (2021). Affinity maturation of SARS-CoV-2 neutralizing antibodies confers potency,
767 breadth, and resilience to viral escape mutations. Immunity.
768 10.1016/j.immuni.2021.07.008.

769 28. Turner, J.S., O'Halloran, J.A., Kalaidina, E., Kim, W., Schmitz, A.J., Zhou, J.Q., Lei,
770 T., Thapa, M., Chen, R.E., Case, J.B., et al. (2021). SARS-CoV-2 mRNA vaccines
771 induce persistent human germinal centre responses. Nature. 10.1038/s41586-021-
772 03738-2.

773 29. Kim, W., Zhou, J.Q., Horvath, S.C., Schmitz, A.J., Sturtz, A.J., Lei, T., Liu, Z.,
774 Kalaidina, E., Thapa, M., Alsoussi, W.B., et al. (2022). Germinal centre-driven
775 maturation of B cell response to mRNA vaccination. Nature, 1–8. 10.1038/s41586-
776 022-04527-1.

777 30. Victora, G.D., and Nussenzweig, M.C. (2022). Germinal centers. Annu. Rev.
778 Immunol. *40*, 413–442. 10.1146/annurev-immunol-120419-022408.

779 31. Seifert, M., Przekopowitz, M., Taudien, S., Lollies, A., Ronge, V., Drees, B.,
780 Lindemann, M., Hillen, U., Engler, H., Singer, B.B., et al. (2015). Functional
781 capacities of human IgM memory B cells in early inflammatory responses and
782 secondary germinal center reactions. Proc. Natl. Acad. Sci. U. S. A. *112*, E546-55.
783 10.1073/pnas.1416276112.

784 32. Dogan, I., Bertocci, B., Vilmont, V., Delbos, F., Mégret, J., Storck, S., Reynaud, C.-
785 A., and Weill, J.-C. (2009). Multiple layers of B cell memory with different effector
786 functions. Nat. Immunol. *10*, 1292–1299. 10.1038/ni.1814.

787 33. Pape, K.A., Taylor, J.J., Maul, R.W., Gearhart, P.J., and Jenkins, M.K. (2011).
788 Different B cell populations mediate early and late memory during an endogenous
789 immune response. Science *331*, 1203–1207. 10.1126/science.1201730.

790 34. Zuccarino-Catania, G.V., Sadanand, S., Weisel, F.J., Tomayko, M.M., Meng, H.,
791 Kleinstein, S.H., Good-Jacobson, K.L., and Shlomchik, M.J. (2014). CD80 and PD-
792 L2 define functionally distinct memory B cell subsets that are independent of
793 antibody isotype. Nat. Immunol. *15*, 631–637. 10.1038/ni.2914.

794 35. Horikawa, K., Martin, S.W., Pogue, S.L., Silver, K., Peng, K., Takatsu, K., and
795 Goodnow, C.C. (2007). Enhancement and suppression of signaling by the
796 conserved tail of IgG memory-type B cell antigen receptors. J. Exp. Med. *204*, 759–
797 769. 10.1084/jem.20061923.

798 36. Waisman, A., Kraus, M., Seagal, J., Ghosh, S., Melamed, D., Song, J., Sasaki, Y.,
799 Classen, S., Lutz, C., Brombacher, F., et al. (2007). IgG1 B cell receptor signaling is
800 inhibited by CD22 and promotes the development of B cells whose survival is less
801 dependent on Ig alpha/beta. J. Exp. Med. *204*, 747–758. 10.1084/jem.20062024.

802 37. Engels, N., König, L.M., Heemann, C., Lutz, J., Tsubata, T., Griep, S., Schrader, V.,
803 and Wienands, J. (2009). Recruitment of the cytoplasmic adaptor Grb2 to surface
804 IgG and IgE provides antigen receptor-intrinsic costimulation to class-switched B
805 cells. Nat. Immunol. *10*, 1018–1025. 10.1038/ni.1764.

806 38. Kometani, K., Nakagawa, R., Shinnakasu, R., Kaji, T., Rybouchkin, A., Moriyama,
807 S., Furukawa, K., Koseki, H., Takemori, T., and Kurosaki, T. (2013). Repression of

808 the transcription factor Bach2 contributes to predisposition of IgG1 memory B cells
809 toward plasma cell differentiation. Immunity *39*, 136–147.
810 10.1016/j.immuni.2013.06.011.

811 39. Bhattacharya, D., Cheah, M.T., Franco, C.B., Hosen, N., Pin, C.L., Sha, W.C., and
812 Weissman, I.L. (2007). Transcriptional profiling of antigen-dependent murine B cell
813 differentiation and memory formation. J. Immunol. *179*, 6808–6819.
814 10.4049/jimmunol.179.10.6808.

815 40. Tomayko, M.M., Anderson, S.M., Brayton, C.E., Sadanand, S., Steinel, N.C.,
816 Behrens, T.W., and Shlomchik, M.J. (2008). Systematic comparison of gene
817 expression between murine memory and naive B cells demonstrates that memory B
818 cells have unique signaling capabilities. J. Immunol. *181*, 27–38.
819 10.4049/jimmunol.181.1.27.

820 41. Wong, R., Belk, J.A., Govero, J., Uhrlaub, J.L., Reinartz, D., Zhao, H., Errico, J.M.,
821 D'Souza, L., Ripperger, T.J., Nikolich-Zugich, J., et al. (2020). Affinity-Restricted
822 Memory B Cells Dominate Recall Responses to Heterologous Flaviviruses.
823 Immunity *53*, 1078-1094.e7. 10.1016/j.immuni.2020.09.001.

824 42. Mesin, L., Schiepers, A., Ersching, J., Barbulescu, A., Cavazzoni, C.B., Angelini, A.,
825 Okada, T., Kurosaki, T., and Victora, G.D. (2020). Restricted clonality and limited
826 germinal center reentry characterize memory B cell reactivation by boosting. Cell
827 *180*, 92-106.e11. 10.1016/j.cell.2019.11.032.

828 43. Purtha, W.E., Tedder, T.F., Johnson, S., Bhattacharya, D., and Diamond, M.S.
829 (2011). Memory B cells, but not long-lived plasma cells, possess antigen
830 specificities for viral escape mutants. J. Exp. Med. *208*, 2599–2606.
831 10.1084/jem.20110740.

832 44. Francis, T. (1960). On the Doctrine of Original Antigenic Sin. Proc. Am. Philos. Soc.
833 *104*, 572–578.

834 45. Worobey, M., Plotkin, S., and Hensley, S.E. (2020). Influenza Vaccines Delivered in
835 Early Childhood Could Turn Antigenic Sin into Antigenic Blessings. Cold Spring
836 Harb. Perspect. Med. *10*. 10.1101/cshperspect.a038471.

837 46. Anderson, E.M., Li, S.H., Awofolaju, M., Eilola, T., Goodwin, E., Bolton, M.J.,
838 Gouma, S., Manzoni, T.B., Hicks, P., Goel, R.R., et al. (2022). SARS-CoV-2
839 infections elicit higher levels of original antigenic sin antibodies compared with
840 SARS-CoV-2 mRNA vaccinations. Cell Rep. *41*, 111496.
841 10.1016/j.celrep.2022.111496.

842 47. Amanat, F., Thapa, M., Lei, T., Sayed Ahmed, S.M., Adelsberg, D.C., Carreno,
843 J.M., Strohmeier, S., Schmitz, A.J., Zafar, S., Zhou, J.Q., et al. (2021). SARS-CoV-
844 2 mRNA vaccination induces functionally diverse antibodies to NTD, RBD and S2.
845 Cell. 10.1016/j.cell.2021.06.005.

846 48. Worobey, M., Han, G.-Z., and Rambaut, A. (2014). Genesis and pathogenesis of
847 the 1918 pandemic H1N1 influenza A virus. Proc. Natl. Acad. Sci. U. S. A. *111*,
848 8107–8112. 10.1073/pnas.1324197111.

849 49. Taubenberger, J.K., and Morens, D.M. (2006). 1918 Influenza: the mother of all
850 pandemics. Emerg. Infect. Dis. *12*, 15–22. 10.3201/eid1201.050979.

851 50. Gostic, K.M., Bridge, R., Brady, S., Viboud, C., Worobey, M., and Lloyd-Smith, J.O.
852 (2019). Childhood immune imprinting to influenza A shapes birth year-specific risk
853 during seasonal H1N1 and H3N2 epidemics. PLoS Pathog. *15*, e1008109.
854 10.1371/journal.ppat.1008109.

855 51. Gostic, K.M., Ambrose, M., Worobey, M., and Lloyd-Smith, J.O. (2016). Potent
856 protection against H5N1 and H7N9 influenza via childhood hemagglutinin
857 imprinting. Science *354*, 722–726. 10.1126/science.aag1322.

858 52. Greaney, A.J., Eguia, R.T., Starr, T.N., Khan, K., Franko, N., Logue, J.K., Lord,
859 S.M., Speake, C., Chu, H.Y., Sigal, A., et al. (2022). The SARS-CoV-2 Delta variant
860 induces an antibody response largely focused on class 1 and 2 antibody epitopes.
861 PLoS Pathog. *18*, e1010592. 10.1371/journal.ppat.1010592.

862 53. Abbott, R.K., Lee, J.H., Menis, S., Skog, P., Rossi, M., Ota, T., Kulp, D.W., Bhullar,
863 D., Kalyuzhniy, O., Havenar-Daughton, C., et al. (2018). Precursor Frequency and
864 Affinity Determine B Cell Competitive Fitness in Germinal Centers, Tested with
865 Germline-Targeting HIV Vaccine Immunogens. Immunity *48*, 133-146.e6.
866 10.1016/j.immuni.2017.11.023.

867 54. Chan, T.D., Gatto, D., Wood, K., Camidge, T., Basten, A., and Brink, R. (2009).
868 Antigen affinity controls rapid T-dependent antibody production by driving the

869 expansion rather than the differentiation or extrafollicular migration of early
870 plasmablasts. J. Immunol. *183*, 3139–3149. 10.4049/jimmunol.0901690.

871 55. Anderson, S.M., Khalil, A., Uduman, M., Hershberg, U., Louzoun, Y., Haberman,
872 A.M., Kleinstein, S.H., and Shlomchik, M.J. (2009). Taking advantage: high-affinity
873 B cells in the germinal center have lower death rates, but similar rates of division,
874 compared to low-affinity cells. J. Immunol. *183*, 7314–7325.
875 10.4049/jimmunol.0902452.

876 56. Shih, T.-A.Y., Meffre, E., Roederer, M., and Nussenzweig, M.C. (2002). Role of
877 BCR affinity in T cell dependent antibody responses in vivo. Nat. Immunol. *3*, 570–
878 575. 10.1038/ni803.

879 57. Yeh, C.-H., Nojima, T., Kuraoka, M., and Kelsoe, G. (2018). Germinal center entry
880 not selection of B cells is controlled by peptide-MHCII complex density. Nat.
881 Commun. *9*, 1–11. 10.1038/s41467-018-03382-x.

882 58. Kwong, P.D., Wyatt, R., Robinson, J., Sweet, R.W., Sodroski, J., and Hendrickson,
883 W.A. (1998). Structure of an HIV gp120 envelope glycoprotein in complex with the
884 CD4 receptor and a neutralizing human antibody. Nature *393*, 648–659.
885 10.1038/31405.

886 59. Grant, O.C., Montgomery, D., Ito, K., and Woods, R.J. (2020). Analysis of the
887 SARS-CoV-2 spike protein glycan shield reveals implications for immune
888 recognition. Sci. Rep. *10*, 14991. 10.1038/s41598-020-71748-7.

889 60. Chan, T.D., Wood, K., Hermes, J.R., Butt, D., Jolly, C.J., Basten, A., and Brink, R.
890 (2012). Elimination of germinal-center-derived self-reactive B cells is governed by
891 the location and concentration of self-antigen. Immunity *37*, 893–904.
892 10.1016/j.immuni.2012.07.017.

893 61. Reed, J.H., Jackson, J., Christ, D., and Goodnow, C.C. (2016). Clonal redemption
894 of autoantibodies by somatic hypermutation away from self-reactivity during human
895 immunization. J. Exp. Med. *213*, 1255–1265. 10.1084/jem.20151978.

896 62. Sabouri, Z., Schofield, P., Horikawa, K., Spierings, E., Kipling, D., Randall, K.L.,
897 Langley, D., Roome, B., Vazquez-Lombardi, R., Rouet, R., et al. (2014).
898 Redemption of autoantibodies on anergic B cells by variable-region glycosylation
899 and mutation away from self-reactivity. Proc. Natl. Acad. Sci. U. S. A. *111*, E2567-
900 75. 10.1073/pnas.1406974111.

901 63. Sangesland, M., Torrents de la Peña, A., Boyoglu-Barnum, S., Ronsard, L.,
902 Mohamed, F.A.N., Moreno, T.B., Barnes, R.M., Rohrer, D., Lonberg, N.,
903 Ghebremichael, M., et al. (2022). Allelic polymorphism controls autoreactivity and
904 vaccine elicitation of human broadly neutralizing antibodies against influenza virus.
905 Immunity *55*, 1693-1709.e8. 10.1016/j.immuni.2022.07.006.

906 64. Berman, J.E., Nickerson, K.G., Pollock, R.R., Barth, J.E., Schuurman, R.K.,
907 Knowles, D.M., Chess, L., and Alt, F.W. (1991). VH gene usage in humans: biased
908 usage of the VH6 gene in immature B lymphoid cells. Eur. J. Immunol. *21*, 1311–
909 1314. 10.1002/eji.1830210532.

910 65. Willems van Dijk, K., Milner, L.A., Sasso, E.H., and Milner, E.C. (1992).
911 Chromosomal organization of the heavy chain variable region gene segments
912 comprising the human fetal antibody repertoire. Proc. Natl. Acad. Sci. U. S. A. *89*,
913 10430–10434. 10.1073/pnas.89.21.10430.

914 66. Nadel, B., Tang, A., Lugo, G., Love, V., Escuro, G., and Feeney, A.J. (1998).
915 Decreased frequency of rearrangement due to the synergistic effect of nucleotide
916 changes in the heptamer and nonamer of the recombination signal sequence of the
917 V kappa gene A2b, which is associated with increased susceptibility of Navajos to
918 Haemophilus influenzae type b disease. J. Immunol. *161*, 6068–6073.

919 67. Murray, S.M., Ansari, A.M., Frater, J., Klenerman, P., Dunachie, S., Barnes, E., and
920 Ogbe, A. (2023). The impact of pre-existing cross-reactive immunity on SARS-CoV-
921 2 infection and vaccine responses. Nat. Rev. Immunol. *23*, 304–316.
922 10.1038/s41577-022-00809-x.

923 68. Chemaitelly, H., Ayoub, H.H., Tang, P., Hasan, M.R., Coyle, P., Yassine, H.M., Al-
924 Khatib, H.A., Smatti, M.K., Al-Kanaani, Z., Al-Kuwari, E., et al. (2022). Immune
925 Imprinting and Protection against Repeat Reinfection with SARS-CoV-2. N. Engl. J.
926 Med. 10.1056/NEJMc2211055.

927 69. Koutsakos, M., and Ellebedy, A.H. (2023). Immunological imprinting: Understanding
928 COVID-19. Immunity *56*, 909–913. 10.1016/j.immuni.2023.04.012.

929 70. Alsoussi, W.B., Malladi, S.K., Zhou, J.Q., Liu, Z., Ying, B., Kim, W., Schmitz, A.J.,
930 Lei, T., Horvath, S.C., Sturtz, A.J., et al. (2023). SARS-CoV-2 Omicron boosting

931 induces de novo B cell response in humans. Nature *617*, 592–598.
932 10.1038/s41586-023-06025-4.

933 71. Cao, Y., Yisimayi, A., Jian, F., Song, W., Xiao, T., Wang, L., Du, S., Wang, J., Li,
934 Q., Chen, X., et al. (2022). BA.2.12.1, BA.4 and BA.5 escape antibodies elicited by
935 Omicron infection. Nature *608*, 593–602. 10.1038/s41586-022-04980-y.

936 72. Cao, Y., Jian, F., Wang, J., Yu, Y., Song, W., Yisimayi, A., Wang, J., An, R., Chen,
937 X., Zhang, N., et al. (2023). Imprinted SARS-CoV-2 humoral immunity induces
938 convergent Omicron RBD evolution. Nature *614*, 521–529. 10.1038/s41586-022-
939 05644-7.

940 73. Park, Y.-J., Pinto, D., Walls, A.C., Liu, Z., De Marco, A., Benigni, F., Zatta, F.,
941 Silacci-Fregni, C., Bassi, J., Sprouse, K.R., et al. (2022). Imprinted antibody
942 responses against SARS-CoV-2 Omicron sublineages. Science *378*, 619–627.
943 10.1126/science.adc9127.

944 74. Reynolds, C.J., Gibbons, J.M., Pade, C., Lin, K.-M., Sandoval, D.M., Pieper, F.,
945 Butler, D.K., Liu, S., Otter, A.D., Joy, G., et al. (2022). Heterologous infection and
946 vaccination shapes immunity against SARS-CoV-2 variants. Science *375*, 183–192.
947 10.1126/science.abm0811.

948 75. Gagne, M., Moliva, J.I., Foulds, K.E., Andrew, S.F., Flynn, B.J., Werner, A.P.,
949 Wagner, D.A., Teng, I.-T., Lin, B.C., Moore, C., et al. (2022). mRNA-1273 or
950 mRNA-Omicron boost in vaccinated macaques elicits similar B cell expansion,

951 neutralizing responses, and protection from Omicron. Cell *185*, 1556-1571.e18.
952 10.1016/j.cell.2022.03.038.

953 76. Masurel, N. (1969). RELATION BETWEEN HONG KONG VIRUS AND FORMER
954 HUMAN A2 ISOLATES AND THE A/EQUI2 VIRUS IN HUMAN SERA COLLECTED
955 BEFORE 1957. Lancet *293*, 907–910. 10.1016/S0140-6736(69)92544-6.

956 77. Masurel, N., and Heijtink, R.A. (1983). Recycling of H1N1 influenza A virus in man--
957 a haemagglutinin antibody study. J. Hyg. *90*, 397–402.
958 10.1017/s0022172400029028.

959 78. Zhang, Z., Mateus, J., Coelho, C.H., Dan, J.M., Moderbacher, C.R., Gálvez, R.I.,
960 Cortes, F.H., Grifoni, A., Tarke, A., Chang, J., et al. (2022). Humoral and cellular
961 immune memory to four COVID-19 vaccines. Cell *185*, 2434-2451.e17.
962 10.1016/j.cell.2022.05.022.

963 79. Kaplonek, P., Fischinger, S., Cizmeci, D., Bartsch, Y.C., Kang, J., Burke, J.S., Shin,
964 S.A., Dayal, D., Martin, P., Mann, C., et al. (2022). mRNA-1273 vaccine-induced
965 antibodies maintain Fc-effector functions across SARS-CoV-2 Variants of Concern.
966 Immunity. 10.1016/j.immuni.2022.01.001.

967 80. Goel, R.R., Apostolidis, S.A., Painter, M.M., Mathew, D., Pattekar, A., Kuthuru, O.,
968 Gouma, S., Hicks, P., Meng, W., Rosenfeld, A.M., et al. (2021). Distinct antibody
969 and memory B cell responses in SARS-CoV-2 naïve and recovered individuals
970 following mRNA vaccination. Sci Immunol *6*. 10.1126/sciimmunol.abi6950.

971 81. Greaney, A.J., Loes, A.N., Gentles, L.E., Crawford, K.H.D., Starr, T.N., Malone,
972 K.D., Chu, H.Y., and Bloom, J.D. (2021). Antibodies elicited by mRNA-1273
973 vaccination bind more broadly to the receptor binding domain than do those from
974 SARS-CoV-2 infection. Science Translational Medicine.
975 10.1126/scitranslmed.abi9915.

976 82. Cherian, S., Potdar, V., Jadhav, S., Yadav, P., Gupta, N., Das, M., Rakshit, P.,
977 Singh, S., Abraham, P., Panda, S., et al. (2021). SARS-CoV-2 spike mutations,
978 L452R, T478K, E484Q and P681R, in the second wave of COVID-19 in
979 Maharashtra, India. Microorganisms *9*, 1542. 10.3390/microorganisms9071542.

980 83. Akinbami, L.J., Kruszon-Moran, D., Wang, C.-Y., Storandt, R.J., Clark, J., Riddles,
981 M.K., and Mohadjer, L.K. (2022). SARS-CoV-2 serology and self-reported infection
982 among adults - National Health and Nutrition Examination Survey, United States,
983 august 2021-may 2022. MMWR Morb. Mortal. Wkly. Rep. *71*, 1522–1525.
984 10.15585/mmwr.mm7148a4.

985 84. Jones, J.M., Manrique, I.M., Stone, M.S., Grebe, E., Saa, P., Germanio, C.D.,
986 Spencer, B.R., Notari, E., Bravo, M., Lanteri, M.C., et al. (2023). Estimates of
987 SARS-CoV-2 seroprevalence and incidence of primary SARS-CoV-2 infections
988 among blood donors, by COVID-19 vaccination status - United States, April 2021-
989 September 2022. MMWR Morb. Mortal. Wkly. Rep. *72*, 601–605.
990 10.15585/mmwr.mm7222a3.

991 85. Lutrick, K., Ellingson, K.D., Baccam, Z., Rivers, P., Beitel, S., Parker, J., Hollister,
992 J., Sun, X., Gerald, J.K., Komatsu, K., et al. (2021). COVID-19 infection, reinfection,

993 and vaccine effectiveness in a prospective cohort of Arizona frontline/essential
994 workers: The AZ HEROES research protocol. JMIR Res. Protoc. *10*, e28925.
995 10.2196/28925.

996 86. Edwards, L.J., Fowlkes, A.L., Wesley, M.G., Kuntz, J.L., Odean, M.J., Caban-
997 Martinez, A.J., Dunnigan, K., Phillips, A.L., Grant, L., Herring, M.K., et al. (2021).
998 "Research on the Epidemiology of SARS-CoV-2 in Essential Response Personnel
999 (RECOVER) Study: Protocol for a multi-site longitudinal cohort." JMIR Res Protoc
1000 *7*.

1001 87. Rambaut, A., Holmes, E.C., O'Toole, Á., Hill, V., McCrone, J.T., Ruis, C., du
1002 Plessis, L., and Pybus, O.G. (2020). A dynamic nomenclature proposal for SARS-
1003 CoV-2 lineages to assist genomic epidemiology. Nat. Microbiol. *5*, 1403–1407.
1004 10.1038/s41564-020-0770-5.

1005 88. Ripperger, T.J., Uhrlaub, J.L., Watanabe, M., Wong, R., Castaneda, Y., Pizzato,
1006 H.A., Thompson, M.R., Bradshaw, C., Weinkauf, C.C., Bime, C., et al. (2020).
1007 Orthogonal SARS-CoV-2 Serological Assays Enable Surveillance of Low-
1008 Prevalence Communities and Reveal Durable Humoral Immunity. Immunity *53*,
1009 925-933.e4. 10.1016/j.immuni.2020.10.004.

1010 89. Piccoli, L., Park, Y.-J., Tortorici, M.A., Czudnochowski, N., Walls, A.C., Beltramello,
1011 M., Silacci-Fregni, C., Pinto, D., Rosen, L.E., Bowen, J.E., et al. (2020). Mapping
1012 Neutralizing and Immunodominant Sites on the SARS-CoV-2 Spike Receptor-
1013 Binding Domain by Structure-Guided High-Resolution Serology. Cell *183*, 1024-
1014 1042.e21. 10.1016/j.cell.2020.09.037.

1015 90. Greaney, A.J., Loes, A.N., Crawford, K.H.D., Starr, T.N., Malone, K.D., Chu, H.Y.,
1016 and Bloom, J.D. (2021). Comprehensive mapping of mutations in the SARS-CoV-2
1017 receptor-binding domain that affect recognition by polyclonal human plasma
1018 antibodies. Cell Host Microbe *29*, 463-476.e6. 10.1016/j.chom.2021.02.003.

1019 91. Röltgen, K., Nielsen, S.C.A., Silva, O., Younes, S.F., Zaslavsky, M., Costales, C.,
1020 Yang, F., Wirz, O.F., Solis, D., Hoh, R.A., et al. (2022). Immune imprinting, breadth
1021 of variant recognition, and germinal center response in human SARS-CoV-2
1022 infection and vaccination. Cell *185*, 1025-1040.e14. 10.1016/j.cell.2022.01.018.

1023 92. Suryadevara, N., Shrihari, S., Gilchuk, P., VanBlargan, L.A., Binshtein, E., Zost,
1024 S.J., Nargi, R.S., Sutton, R.E., Winkler, E.S., Chen, E.C., et al. (2021). Neutralizing
1025 and protective human monoclonal antibodies recognizing the N-terminal domain of
1026 the SARS-CoV-2 spike protein. Cell *184*, 2316-2331.e15.
1027 10.1016/j.cell.2021.03.029.

1028 93. Cerutti, G., Guo, Y., Zhou, T., Gorman, J., Lee, M., Rapp, M., Reddem, E.R., Yu, J.,
1029 Bahna, F., Bimela, J., et al. (2021). Potent SARS-CoV-2 neutralizing antibodies
1030 directed against spike N-terminal domain target a single supersite. Cell Host
1031 Microbe *29*, 819-833.e7. 10.1016/j.chom.2021.03.005.

1032 94. McCallum, M., De Marco, A., Lempp, F.A., Tortorici, M.A., Pinto, D., Walls, A.C.,
1033 Beltramello, M., Chen, A., Liu, Z., Zatta, F., et al. (2021). N-terminal domain
1034 antigenic mapping reveals a site of vulnerability for SARS-CoV-2. Cell *184*, 2332-
1035 2347.e16. 10.1016/j.cell.2021.03.028.

1036 95. Shroff, R.T., Chalasani, P., Wei, R., Pennington, D., Quirk, G., Schoenle, M.V.,
1037 Peyton, K.L., Uhrlaub, J.L., Ripperger, T.J., Jergović, M., et al. (2021). Immune
1038 responses to two and three doses of the BNT162b2 mRNA vaccine in adults with
1039 solid tumors. Nat. Med., 1–10. 10.1038/s41591-021-01542-z.

1040 96. Motozono, C., Toyoda, M., Zahradnik, J., Saito, A., Nasser, H., Tan, T.S., Ngare, I.,
1041 Kimura, I., Uriu, K., Kosugi, Y., et al. (2021). SARS-CoV-2 spike L452R variant
1042 evades cellular immunity and increases infectivity. Cell Host Microbe.
1043 10.1016/j.chom.2021.06.006.

1044 97. He, P., Liu, B., Gao, X., Yan, Q., Pei, R., Sun, J., Chen, Q., Hou, R., Li, Z., Zhang,
1045 Y., et al. (2022). SARS-CoV-2 Delta and Omicron variants evade population
1046 antibody response by mutations in a single spike epitope. Nat Microbiol.
1047 10.1038/s41564-022-01235-4.

1048 98. Tchesnokova, V., Kulasekara, H., Larson, L., Bowers, V., Rechkina, E., Kisiela, D.,
1049 Sledneva, Y., Choudhury, D., Maslova, I., Deng, K., et al. (2021). Acquisition of the
1050 L452R mutation in the ACE2-binding interface of spike protein triggers recent
1051 massive expansion of SARS-CoV-2 variants. J. Clin. Microbiol. *59*, e0092121.
1052 10.1128/JCM.00921-21.

1053 99. Greaney, A.J., Starr, T.N., Eguia, R.T., Loes, A.N., Khan, K., Karim, F., Cele, S.,
1054 Bowen, J.E., Logue, J.K., Corti, D., et al. (2022). A SARS-CoV-2 variant elicits an
1055 antibody response with a shifted immunodominance hierarchy. PLoS Pathog. *18*,
1056 e1010248. 10.1371/journal.ppat.1010248.

1057 100. Setliff, I., Shiakolas, A.R., Pilewski, K.A., Murji, A.A., Mapengo, R.E., Janowska,
1058 K., Richardson, S., Oosthuysen, C., Raju, N., Ronsard, L., et al. (2019). High-
1059 Throughput Mapping of B Cell Receptor Sequences to Antigen Specificity. Cell *179*,
1060 1636-1646.e15. 10.1016/j.cell.2019.11.003.

1061 101. Schiepers, A., van ’t Wout, M.F.L., Greaney, A.J., Zang, T., Muramatsu, H., Lin,
1062 P.J.C., Tam, Y.K., Mesin, L., Starr, T.N., Bieniasz, P.D., et al. (2023). Molecular
1063 fate-mapping of serum antibody responses to repeat immunization. Nature.
1064 10.1038/s41586-023-05715-3.

1065 102. Smith, K.G., Light, A., Nossal, G.J., and Tarlinton, D.M. (1997). The extent of
1066 affinity maturation differs between the memory and antibody-forming cell
1067 compartments in the primary immune response. EMBO J. *16*, 2996–3006.
1068 10.1093/emboj/16.11.2996.

1069 103. Lavinder, J.J., Wine, Y., Giesecke, C., Ippolito, G.C., Horton, A.P., Lungu, O.I.,
1070 Hoi, K.H., DeKosky, B.J., Murrin, E.M., Wirth, M.M., et al. (2014). Identification and
1071 characterization of the constituent human serum antibodies elicited by vaccination.
1072 Proc. Natl. Acad. Sci. U. S. A. *111*, 2259–2264. 10.1073/pnas.1317793111.

1073 104. Pape, K.A., Maul, R.W., Dileepan, T., Paustian, A.S., Gearhart, P.J., and
1074 Jenkins, M.K. (2018). Naive B cells with high-avidity germline-encoded antigen
1075 receptors produce persistent IgM+ and transient IgG+ memory B cells. Immunity *48*,
1076 1135-1143.e4. 10.1016/j.immuni.2018.04.019.

1077 105. Andrews, S.F., Kaur, K., Pauli, N.T., Huang, M., Huang, Y., and Wilson, P.C.
1078 (2015). High preexisting serological antibody levels correlate with diversification of
1079 the influenza vaccine response. J. Virol. *89*, 3308–3317. 10.1128/JVI.02871-14.

1080 106. Inoue, T., Shinnakasu, R., Kawai, C., Yamamoto, H., Sakakibara, S., Ono, C.,
1081 Itoh, Y., Terooatea, T., Yamashita, K., Okamoto, T., et al. (2023). Antibody
1082 feedback contributes to facilitating the development of Omicron-reactive memory B
1083 cells in SARS-CoV-2 mRNA vaccinees. J. Exp. Med. *220*. 10.1084/jem.20221786.

1084 107. Liu, Y.J., Zhang, J., Lane, P.J., Chan, E.Y., and MacLennan, I.C. (1991). Sites of
1085 specific B cell activation in primary and secondary responses to T cell-dependent
1086 and T cell-independent antigens. Eur. J. Immunol. *21*, 2951–2962.
1087 10.1002/eji.1830211209.

1088 108. Abbott, R.K., and Crotty, S. (2020). Factors in B cell competition and
1089 immunodominance. Immunol. Rev. *296*, 120–131. 10.1111/imr.12861.

1090 109. Krammer, F. (2019). The human antibody response to influenza A virus infection
1091 and vaccination. Nat. Rev. Immunol. *19*, 383–397. 10.1038/s41577-019-0143-6.

1092 110. Chia, P.Y., Ong, S.W.X., Chiew, C.J., Ang, L.W., Chavatte, J.-M., Mak, T.-M.,
1093 Cui, L., Kalimuddin, S., Chia, W.N., Tan, C.W., et al. (2022). Virological and
1094 serological kinetics of SARS-CoV-2 Delta variant vaccine breakthrough infections: a
1095 multicentre cohort study. Clin. Microbiol. Infect. *28*, 612.e1-612.e7.
1096 10.1016/j.cmi.2021.11.010.

1097 111. Schaefer-Babajew, D., Wang, Z., Muecksch, F., Cho, A., Loewe, M., Cipolla, M.,
1098 Raspe, R., Johnson, B., Canis, M., DaSilva, J., et al. (2023). Antibody feedback
1099 regulates immune memory after SARS-CoV-2 mRNA vaccination. Nature *613*, 735–
1100 742. 10.1038/s41586-022-05609-w.

1101 112. Gao, Y., Cai, C., Grifoni, A., Müller, T.R., Niessl, J., Olofsson, A., Humbert, M.,
1102 Hansson, L., Österborg, A., Bergman, P., et al. (2022). Ancestral SARS-CoV-2-
1103 specific T cells cross-recognize the Omicron variant. Nat. Med. *28*, 472–476.
1104 10.1038/s41591-022-01700-x.

1105 113. Keeton, R., Tincho, M.B., Ngomti, A., Baguma, R., Benede, N., Suzuki, A., Khan,
1106 K., Cele, S., Bernstein, M., Karim, F., et al. (2022). T cell responses to SARS-CoV-2
1107 spike cross-recognize Omicron. Nature *603*, 488–492. 10.1038/s41586-022-04460-
1108 3.

1109 114. Bartsch, Y.C., Wang, C., Zohar, T., Fischinger, S., Atyeo, C., Burke, J.S., Kang,
1110 J., Edlow, A.G., Fasano, A., Baden, L.R., et al. (2021). Humoral signatures of
1111 protective and pathological SARS-CoV-2 infection in children. Nat. Med. *27*, 454–
1112 462. 10.1038/s41591-021-01263-3.

1113 115. Ying, B., Scheaffer, S.M., Whitener, B., Liang, C.-Y., Dmytrenko, O., Mackin, S.,
1114 Wu, K., Lee, D., Avena, L.E., Chong, Z., et al. (2022). Boosting with Omicron-
1115 matched or historical mRNA vaccines increases neutralizing antibody responses
1116 and protection against B.1.1.529 infection in mice. bioRxivorg, 2022.02.07.479419.
1117 10.1101/2022.02.07.479419.

1118 116. Barnes, C.O., West, A.P., Jr, Huey-Tubman, K.E., Hoffmann, M.A.G., Sharaf,
1119 N.G., Hoffman, P.R., Koranda, N., Gristick, H.B., Gaebler, C., Muecksch, F., et al.
1120 (2020). Structures of Human Antibodies Bound to SARS-CoV-2 Spike Reveal
1121 Common Epitopes and Recurrent Features of Antibodies. Cell *182*, 828-842.e16.
1122 10.1016/j.cell.2020.06.025.

1123 117. Hay, J.A., Kissler, S.M., Fauver, J.R., Mack, C., Tai, C.G., Samant, R.M.,
1124 Connolly, S., Anderson, D.J., Khullar, G., MacKay, M., et al. (2022). Quantifying the
1125 impact of immune history and variant on SARS-CoV-2 viral kinetics and infection
1126 rebound: A retrospective cohort study. Elife *11*. 10.7554/eLife.81849.

1127 118. Goldfarb, D.M., Tilley, P., Al-Rawahi, G.N., Srigley, J.A., Ford, G., Pedersen, H.,
1128 Pabbi, A., Hannam-Clark, S., Charles, M., Dittrick, M., et al. (2020). Self-collected
1129 saline gargle samples as an alternative to healthcare worker collected
1130 nasopharyngeal swabs for COVID-19 diagnosis in outpatients. J. Clin. Microbiol.,
1131 2020.09.13.20188334. 10.1101/2020.09.13.20188334.

1132 119. Hao, Y., Hao, S., Andersen-Nissen, E., Mauck, W.M., 3rd, Zheng, S., Butler, A.,
1133 Lee, M.J., Wilk, A.J., Darby, C., Zager, M., et al. (2021). Integrated analysis of
1134 multimodal single-cell data. Cell *184*, 3573-3587.e29. 10.1016/j.cell.2021.04.048.

Figure 1

A.

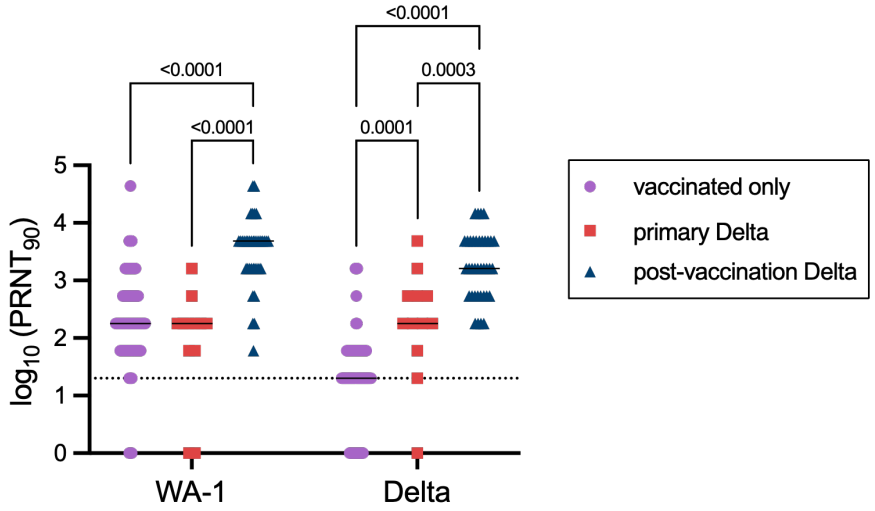
log10 (PRNT90)
5
4
3
2
1
0
<0.0001
<0.0001
<0.0001
0.0003
0.0001
WA-1
Delta
vaccinated only
primary Delta
post-vaccination Delta

B.

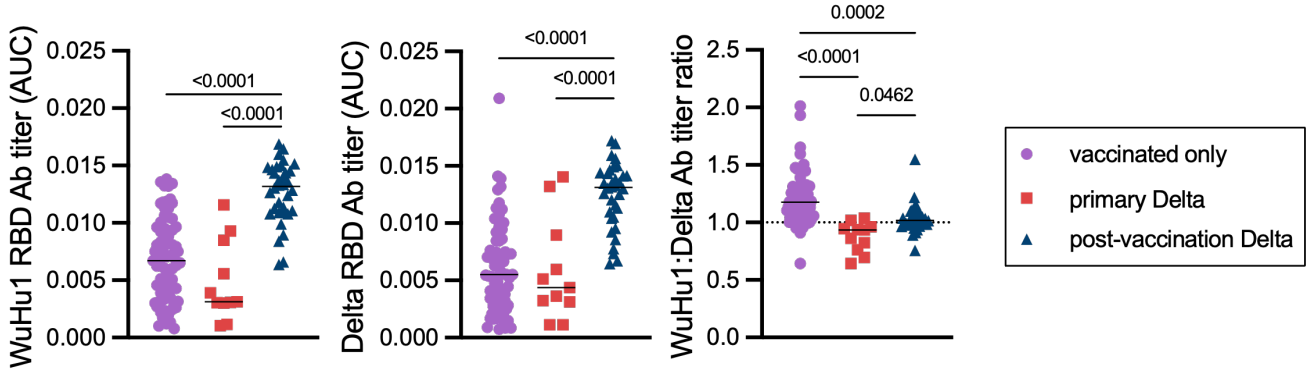
WuHu1 RBD Ab titer (AUC)
0.025
0.020
0.015
0.010
0.005
0.000
<0.0001
<0.0001
Delta RBD Ab titer (AUC)
<0.0001
<0.0001
WuHu1:Delta Ab titer ratio
2.5
2.0
1.5
1.0
0.5
0.0
0.0002
<0.0001
0.0462
vaccinated only
primary Delta
post-vaccination Delta

1135 **Figure 1. Primary and recall antibody responses to Wuhan and Delta strains of**
1136 **SARS-COV-2. (A)** Virus neutralization assays were performed using the WA-1 and
1137 Delta isolates of SARS-CoV-2. Serial 1:3 dilutions of serums were performed and tested
1138 for the ability to prevent plaque formation on Vero cells. The lowest concentration
1139 capable of preventing more than 90% of plaques was considered to be the $PRNT_{90}$
1140 value. Each symbol represents an individual. Two-sided P values from t-test statistics
1141 were calculated for pairwise differences using two-way ANOVA. Post hoc testing for
1142 multiple comparisons between draws was performed using Tukey's multiple
1143 comparisons test. P values greater than 0.05 are not depicted. (**B)** Quantitative titers of
1144 WuHu1- and Delta RBD-specific antibodies. Serum was initially diluted 1:60, serially
1145 diluted 1:3, assessed by ELISA for binding to the listed antigens, and area under the
1146 curve (AUC) values were calculated. Each symbol represents an individual. WuHu1
1147 AUC values were divided by their Delta AUC titer in the same individual to calculate a
1148 WuHu1:Delta RBD ratio in the rightmost panel. Two-sided P values from t-test statistics
1149 were calculated for pairwise differences using one-way ANOVA. Post hoc testing for
1150 multiple comparisons between draws was performed using Tukey's multiple
1151 comparisons test. P values greater than 0.05 are not depicted.
1152
1153

Figure 2

A.

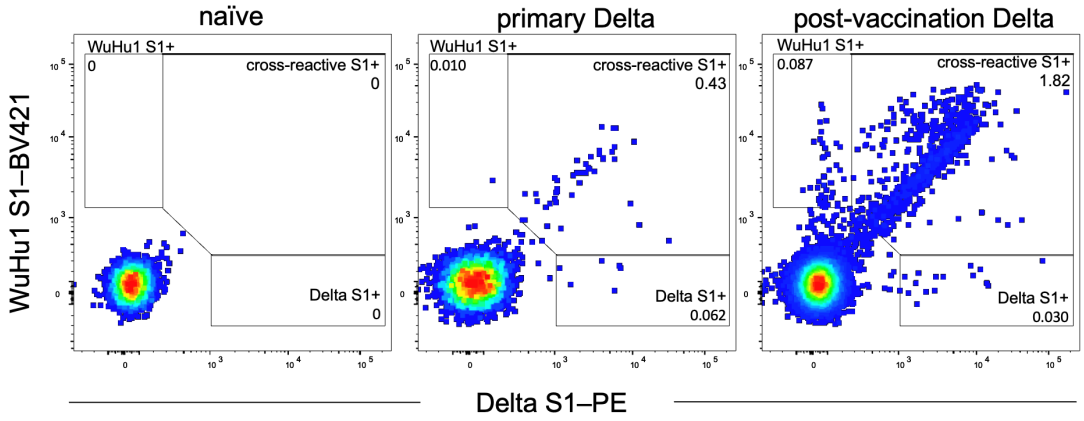
naïve
primary Delta
post-vaccination Delta
WuHu1 S1+
cross-reactive S1+
Delta S1+
0
0.010
0.087
0.43
1.82
0.062
0.030
WuHu1 S1–BV421
Delta S1–PE

B.

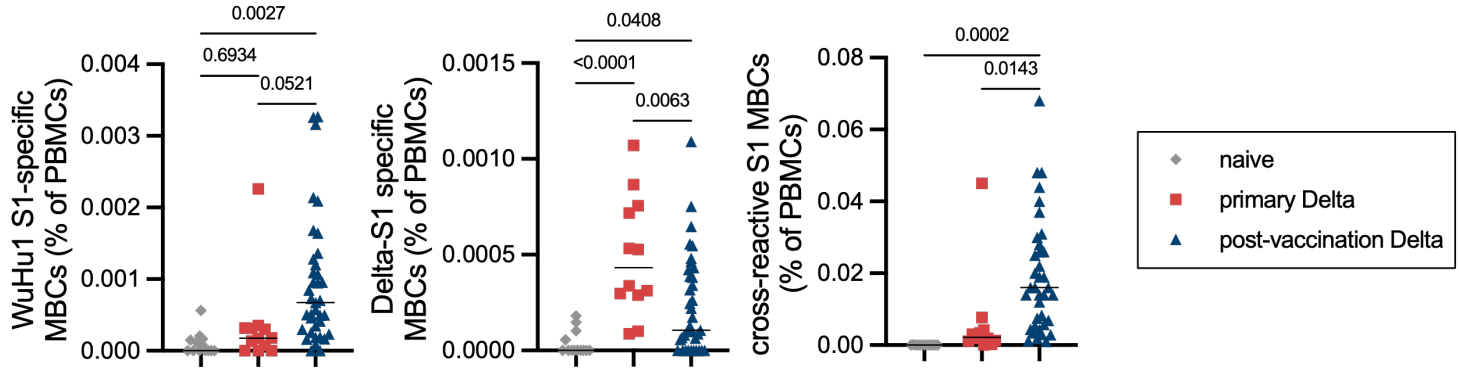
WuHu1 S1-specific MBCs (% of PBMCs)
Delta-S1 specific MBCs (% of PBMCs)
cross-reactive S1 MBCs (% of PBMCs)
0.0027
0.6934
0.0521
0.0408
<0.0001
0.0063
0.0002
0.0143
naive
primary Delta
post-vaccination Delta

C.

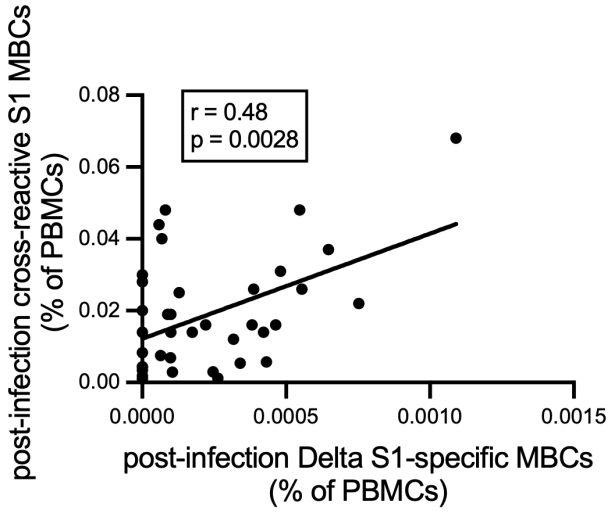
r = 0.48
p = 0.0028
post-infection cross-reactive S1 MBCs (% of PBMCs)
post-infection Delta S1-specific MBCs (% of PBMCs)

1154 **Figure 2. WuHu1 and Delta Memory B cell flow cytometric analysis and**
1155 **quantification. (A)** Representative flow cytometric plots of Wuhu1 and Delta S1-
1156 specific memory B cells (full gating strategy shown in Figure S2) in naïve, primary Delta
1157 infection, and post-vaccination Delta infection cohorts. Cells that bind both WuHu1 S1
1158 and Delta S1 are annotated as cross-reactive S1+, whereas cells that bind only WuHu1
1159 S1 or Delta S1 are annotated as WuHu1 S1+ or Delta S1+, respectively. **(B)**
1160 Quantification of isotype-switched memory B cells as a percentage of total PBMCs for
1161 Wuhu1 S1+, Delta S1+ and cross-reactive S1+ specificities for each cohort of SARS-
1162 CoV-2 immune histories. Each symbol represents an individual. Two-sided P values
1163 from t-test statistics were calculated for pairwise differences using one-way ANOVA.
1164 Post hoc testing for multiple comparisons between draws was performed using Tukey's
1165 multiple comparisons test. P values greater than 0.05 are not depicted. **(C)** Correlation
1166 of post-infection cross-reactive S1 MBCs (calculated as in Figure 2B) plotted against the
1167 frequency of post-infection Delta S1-specific MBCs (calculated as in Figure 2B) in
1168 individuals that experienced a post-vaccination Delta infection. Pearson correlation
1169 analysis was performed.
1170
1171

Figure 3

A.

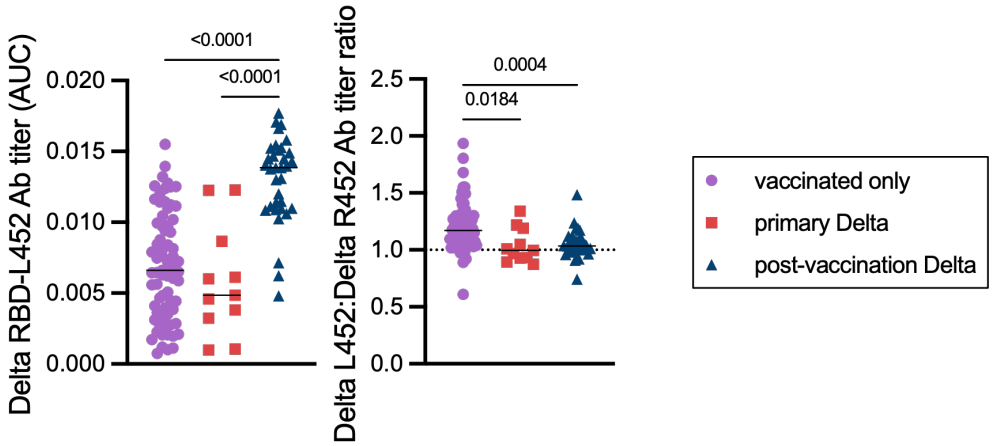

B.

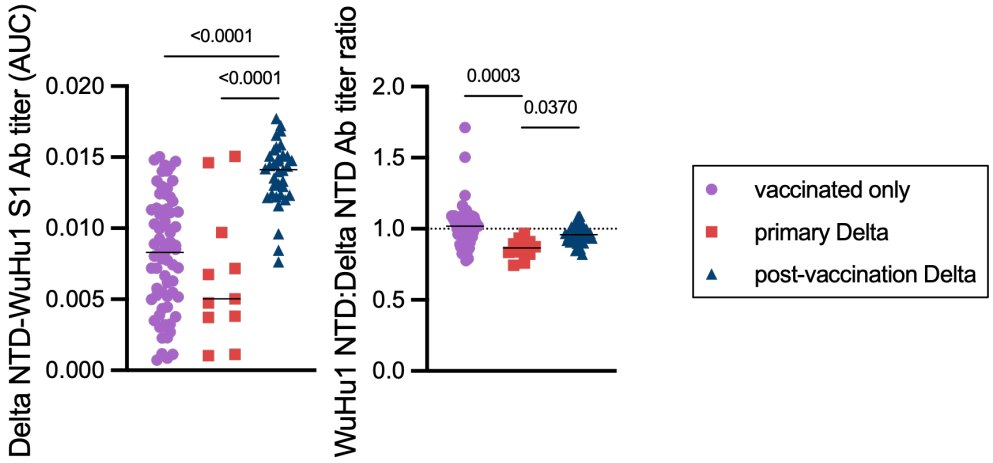

C.

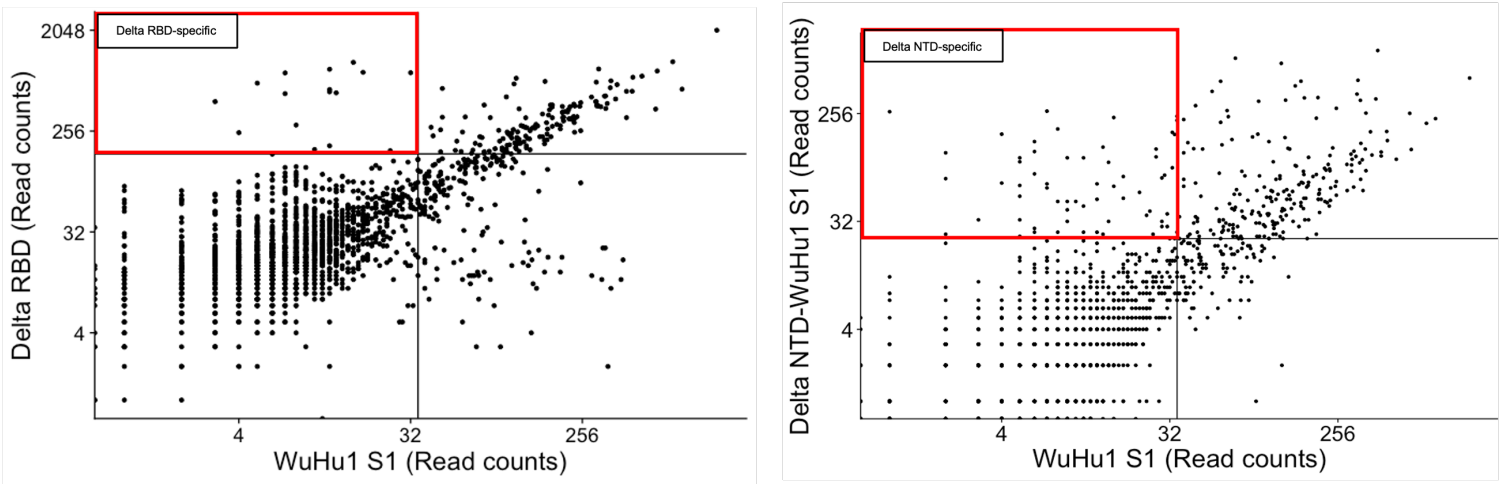

D.

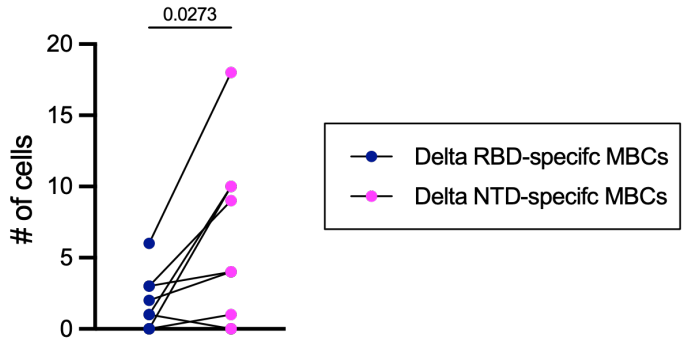

1172 **Figure 3. Epitope-specific quantification of Delta RBD- and Delta NTD-specific**
1173 **antibodies and memory B cells.** (**A)** A chimeric protein (Delta RBD-L452) was
1174 generated in which R452 was reverted to the ancestral L452. ELISAs were used to
1175 quantify serum antibodies that bound to Delta RBD-L452 in each cohort. Delta RBD-
1176 L452 AUC titers were divided by Delta RBD titers (Figure 1B) in the same individuals to
1177 calculate a L452:R452 titer ratio. Each symbol represents an individual. Two-sided P
1178 values from t-test statistics were calculated for pairwise differences using one-way
1179 ANOVA. Post hoc testing for multiple comparisons between draws was performed using
1180 Tukey's multiple comparisons test. P values greater than 0.05 are not depicted. **(B)** A
1181 chimeric protein (Delta NTD-WuHu1 S1) was generated in which Delta NTD mutated
1182 epitopes (T19R, G142D, E156-, F157-, R158G) were incorporated into the otherwise
1183 WuHu1 S1 backbone. ELISAs were used to quantify serum antibodies that bound to
1184 Delta NTD-WuHu1 S1 in each cohort. Delta RBD-L452 AUC titers were divided by their
1185 Delta RBD (Supplemental Fig 1A) titer to calculate a WuHu1 NTD:Delta NTD titer ratio.
1186 Each symbol represents an individual. Two-sided P values from t-test statistics were
1187 calculated for pairwise differences using one-way ANOVA. Post hoc testing for multiple
1188 comparisons between draws was performed using Tukey's multiple comparisons test. P
1189 values greater than 0.05 are not depicted. **(C)** LIBRA-seq plots of isotype-switched
1190 memory B cells enriched for Spike-binding specificities from primary Delta infections.
1191 Read count thresholds to determine positivity were set using samples in which cells
1192 lacking Spike-binding specificities were sorted and sequenced. Plots are concatenated
1193 from ten individuals. **(D)** Quantification of Delta RBD-specific and Delta NTD-specific
1194 memory B cells (MBCs) in individuals that experienced a primary Delta infection. Lines

1195 connect specificities within the same individual. Delta RBD-specific cells were classified
1196 by cells that had Delta RBD read counts of greater than 160 and WuHu1 S1 read
1197 counts of less than 35. Delta NTD-specific cells were classified by cells that had Delta
1198 NTD-WuHu1 S1 read counts of greater than 23 and WuHu1 S1 read counts of less than
1199 35. Two-sided P values were calculated for pairwise differences using paired t-tests.
1200
1201
1202
1203
1204

Figure 4

A.

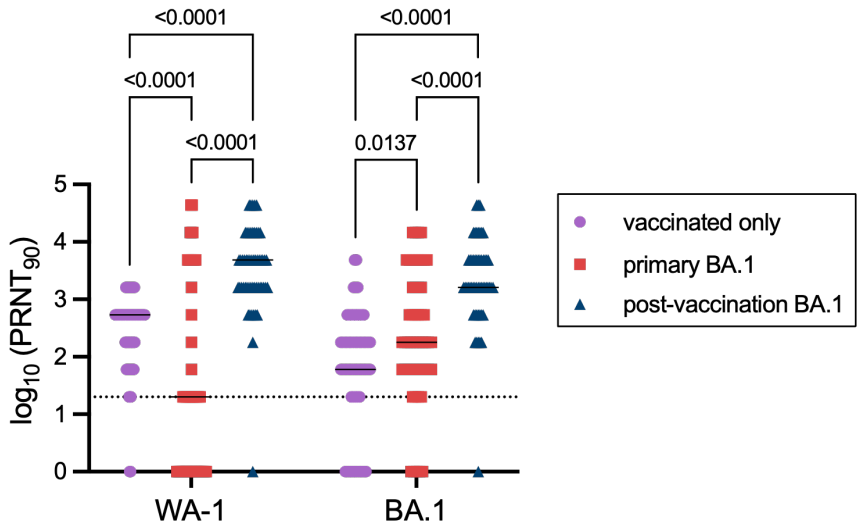
log10 (PRNT90)
WA-1
BA.1
<0.0001
<0.0001
<0.0001
<0.0001
<0.0001
0.0137
vaccinated only
primary BA.1
post-vaccination BA.1

B.

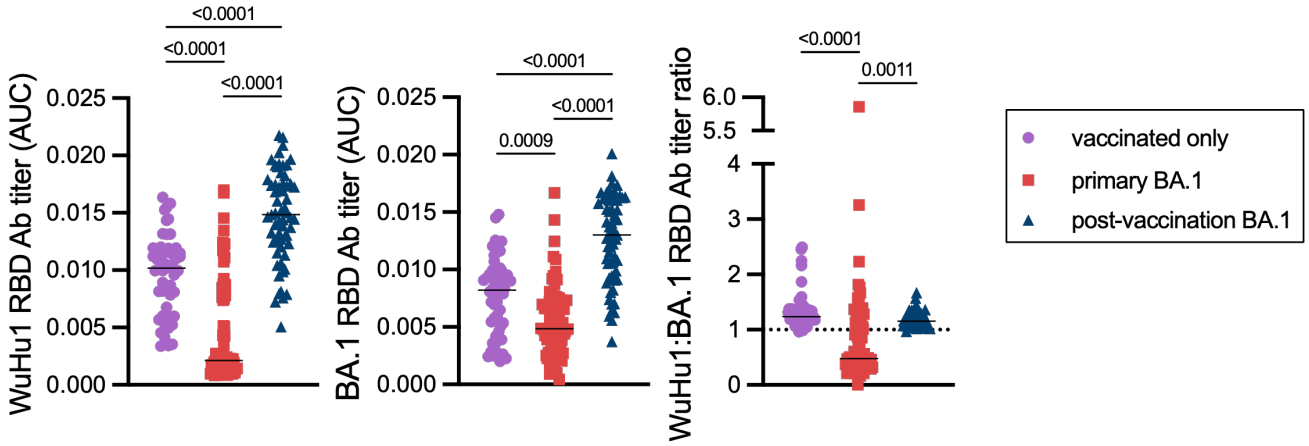
WuHu1 RBD Ab titer (AUC)
BA.1 RBD Ab titer (AUC)
WuHu1:BA.1 RBD Ab titer ratio
<0.0001
<0.0001
<0.0001
<0.0001
<0.0001
0.0009
<0.0001
0.0011
vaccinated only
primary BA.1
post-vaccination BA.1

1205 **Figure 4. Primary and recall antibody responses to Wuhan and BA.1 strains of**
1206 **SARS-COV-2. (A)** Virus neutralization assays were performed using the WA-1 and
1207 BA.1 isolates of SARS-CoV-2. Serial 1:3 dilutions of serums were performed and tested
1208 for the ability to prevent plaque formation on Vero cells. The lowest concentration
1209 capable of preventing more than 90% of plaques was considered to the $PRNT_{90}$ value.
1210 Each symbol represents an individual. Two-sided P values from t-test statistics were
1211 calculated for pairwise differences using two-way ANOVA. Post hoc testing for multiple
1212 comparisons between draws was performed using Tukey's multiple comparisons test. P
1213 values greater than 0.05 are not depicted. **(B)** Quantitative titers of Wuhu1 and BA.1
1214 RBD antibodies. Serum was initially diluted 1:60, serially diluted 1:3, assessed by
1215 ELISA for binding to the listed antigens, and area under the curve (AUC) values were
1216 calculated. Each symbol represents an individual. WuHu1 AUC values were divided by
1217 their BA.1 RBD AUC titer in the same individual to calculate a ratio in the rightmost
1218 panel. Two-sided P values from t-test statistics were calculated for pairwise differences
1219 using one-way ANOVA. Post hoc testing for multiple comparisons between draws was
1220 performed using Tukey's multiple comparisons test. P values greater than 0.05 are not
1221 depicted.
1222
1223

Figure 5

A.

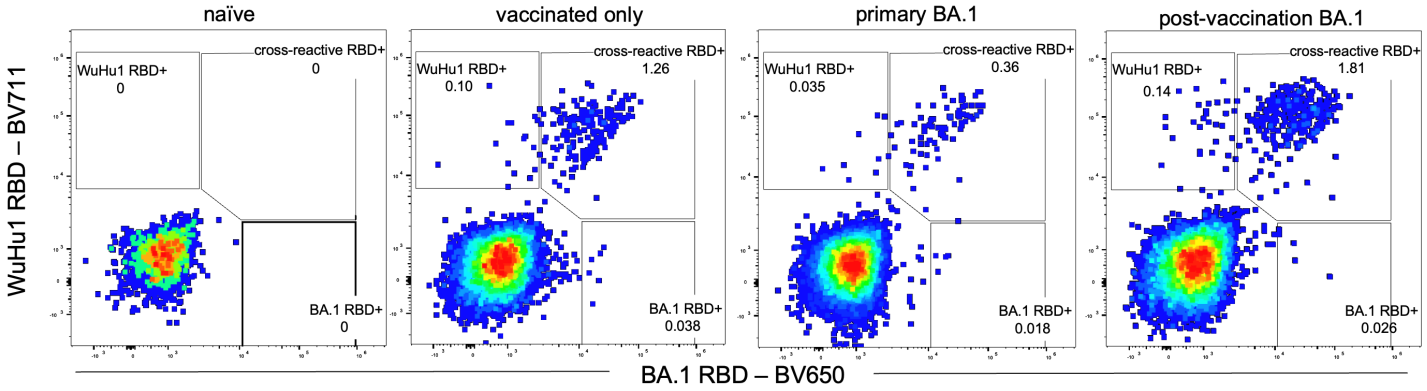

B.

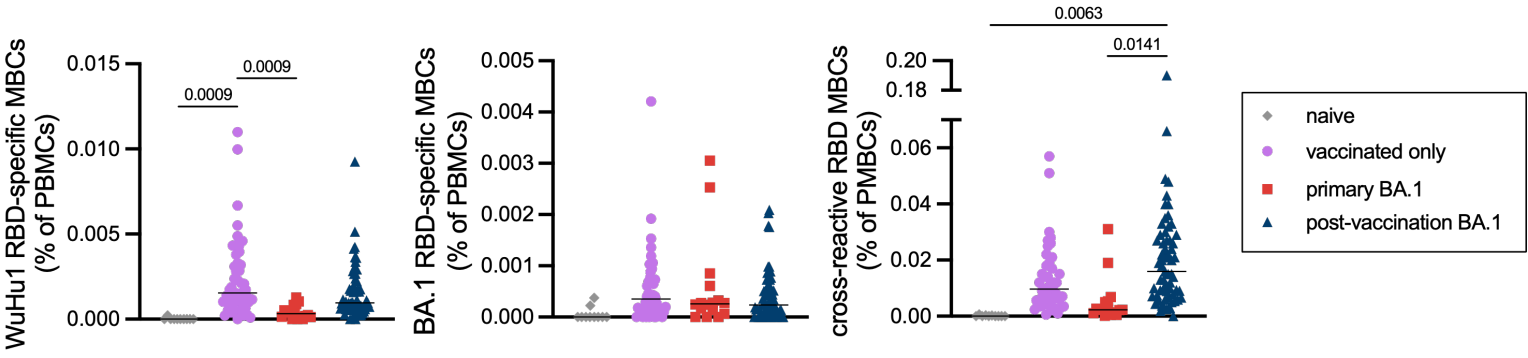

C.

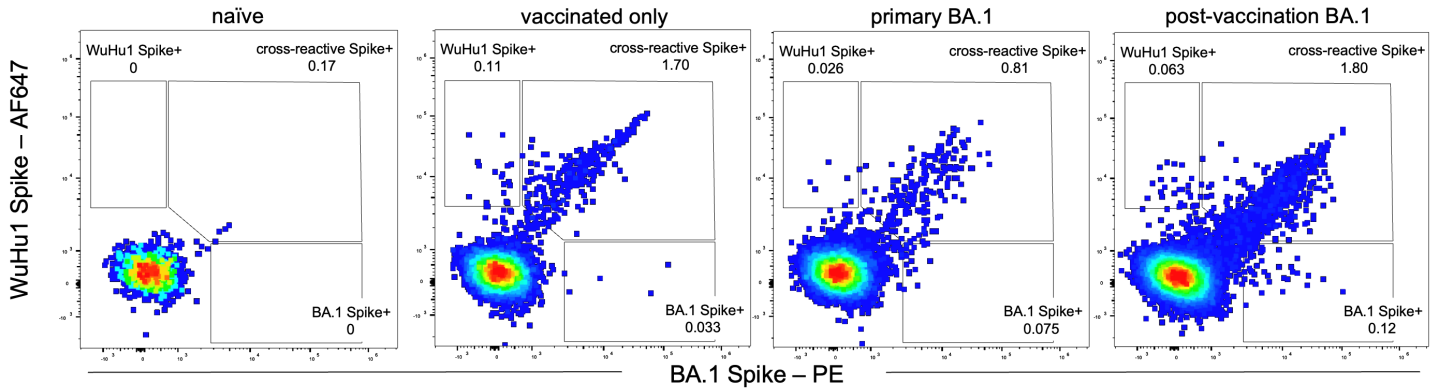

D.

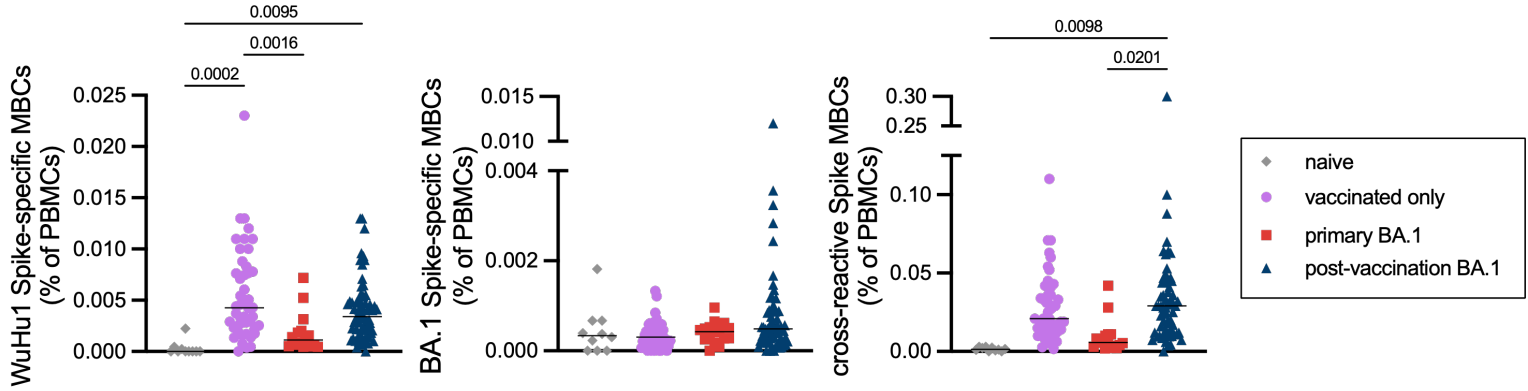

1224 **Figure 5. WuHu1 and BA.1 Memory B cell flow cytometric analysis and**
1225 **quantification. (A)** Representative flow cytometric plots of Wuhu1 and BA.1 RBD-
1226 specific memory B cells (full gating strategy shown in Figure S3) in naïve, vaccinated
1227 only, primary BA.1 infection, and post-vaccination BA.1 infection cohorts. Cells that bind
1228 both WuHu1 RBD and BA.1 RBD are annotated as cross-reactive RBD+, whereas cells
1229 that bind only WuHu1 RBD or BA.1 RBD are annotated as WuHu1 RBD+ or BA.1
1230 RBD+, respectively. **(B)** Quantification of isotype-switched memory B cells for Wuhu1
1231 RBD+, BA.1 RBD+ and cross-reactive RBD+ specificities for each cohort of SARS-CoV-
1232 2 immune histories. Each symbol represents an individual. Two-sided P values from t-
1233 test statistics were calculated for pairwise differences using one-way ANOVA. Post hoc
1234 testing for multiple comparisons between draws was performed using Tukey's multiple
1235 comparisons test. P values greater than 0.05 are not depicted. **(C)** Representative flow
1236 cytometric plots of Wuhu1 and BA.1 Spike-specific memory B cells (full gating strategy
1237 shown in Figure S3) in naïve, vaccinated only, primary BA.1 infection, and post-
1238 vaccination BA.1 infection cohorts. Cells that bind both WuHu1 RBD and BA.1 Spike
1239 are annotated as cross-reactive Spike+, whereas cells that bind only WuHu1 Spike or
1240 BA.1 Spike are annotated as WuHu1 Spike+ or BA.1 Spike+, respectively. **(D)**
1241 Quantification of isotype-switched memory B cells for Wuhu1 Spike+, BA.1 Spike+ and
1242 cross-reactive Spike+ specificities for each cohort of SARS-CoV-2 immune histories.
1243 Each symbol represents an individual. Two-sided P values from t-test statistics were
1244 calculated for pairwise differences using one-way ANOVA. Post hoc testing for multiple
1245 comparisons between draws was performed using Tukey's multiple comparisons test. P
1246 values greater than 0.05 are not depicted.

Figure 6

A.

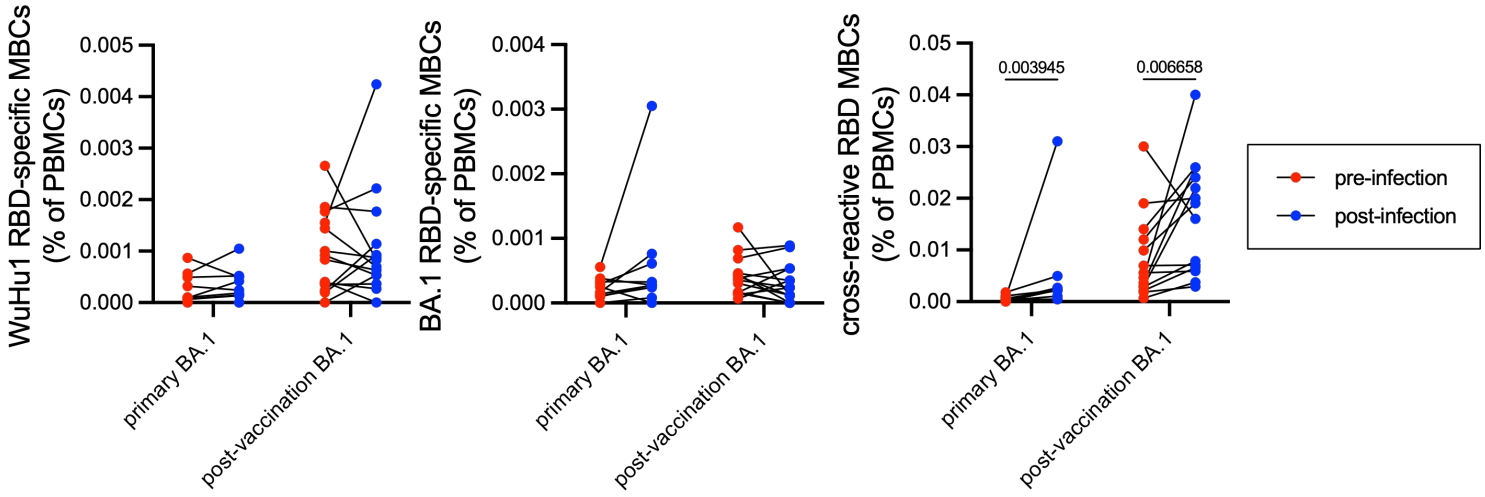
WuHu1 RBD-specific MBCs (% of PBMCs)
0.005
0.004
0.003
0.002
0.001
0.000
primary BA.1
post-vaccination BA.1
BA.1 RBD-specific MBCs (% of PBMCs)
0.004
0.003
0.002
0.001
0.000
primary BA.1
post-vaccination BA.1
cross-reactive RBD MBCs (% of PBMCs)
0.05
0.04
0.03
0.02
0.01
0.00
0.003945
0.006658
primary BA.1
post-vaccination BA.1
pre-infection
post-infection

B.

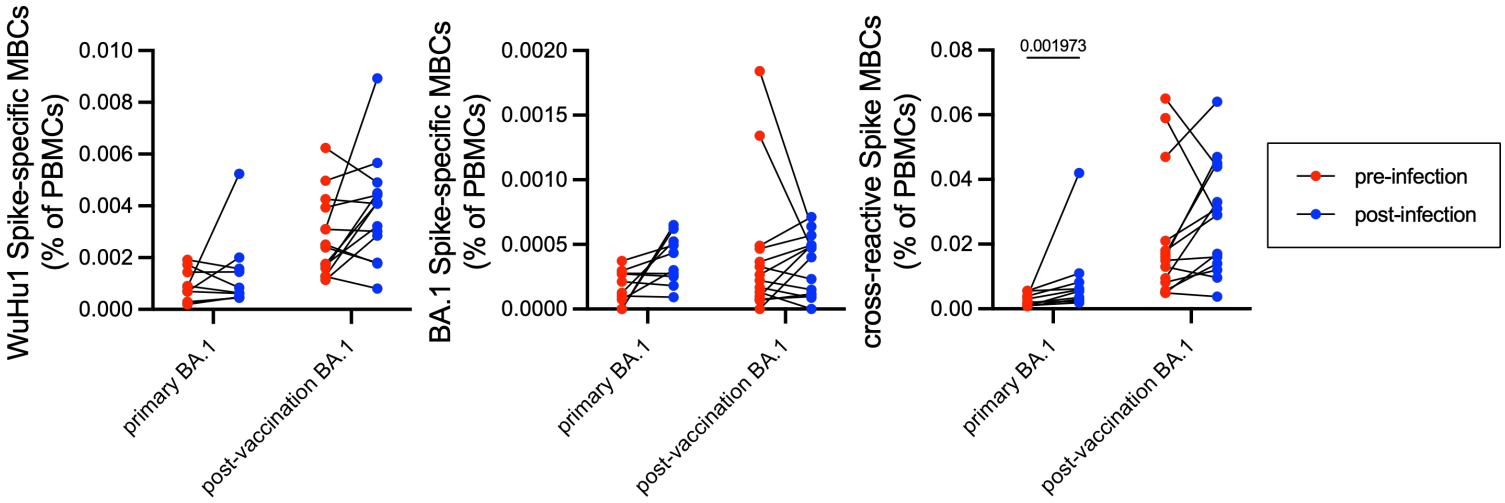
WuHu1 Spike-specific MBCs (% of PBMCs)
0.010
0.008
0.006
0.004
0.002
0.000
primary BA.1
post-vaccination BA.1
BA.1 Spike-specific MBCs (% of PBMCs)
0.0020
0.0015
0.0010
0.0005
0.0000
primary BA.1
post-vaccination BA.1
cross-reactive Spike MBCs (% of PBMCs)
0.08
0.06
0.04
0.02
0.00
0.001973
primary BA.1
post-vaccination BA.1
pre-infection
post-infection

1247 **Figure 6. Frequency of WuHu1- and BA.1-specific memory B cells before and after**
1248 **BA.1 infection. (A)** Frequencies of isotype-switched memory B cells with Wuhu1
1249 RBD+, BA.1 RBD+ and cross-reactive RBD+ specificities in both unvaccinated and
1250 vaccinated individuals before and after BA.1 infection. Lines connect the same
1251 individual from pre-infection frequency to post-infection frequency. In primary infections,
1252 pre-infection blood draws were taken on average 75.6 days before infection and post-
1253 infection blood draws occurred on 37.8 days after infection. In post-vaccination
1254 infections, pre-infection blood draws were taken on average 87.6 days before infection
1255 and post-infection draws were taken an average of 38.3 days after infection. Individuals
1256 that received a vaccine after the pre-infection draw were excluded from analysis. P
1257 values were calculated using Wilcoxon matched-pairs signed rank test on each row and
1258 post hoc testing for multiple comparisons between draws was performed using two-
1259 stage linear step-up procedure of Benjamini, Krieger and Yekutieli. P values greater
1260 than 0.05 are not depicted. **(B)** Frequencies of isotype-switched memory B cells with
1261 Wuhu1 Spike+, BA.1 Spike+ and cross-reactive Spike+ specificities in both
1262 unvaccinated and vaccinated individuals before and after BA.1 infection. Lines connect
1263 the same individual from pre-infection frequency to post-infection frequency. P values
1264 were calculated using Wilcoxon matched-pairs signed rank test on each row and post
1265 hoc testing for multiple comparisons between draws was performed using two-stage
1266 linear step-up procedure of Benjamini, Krieger and Yekutieli. P values greater than 0.05
1267 are not depicted.
1268
1269

Figure 7

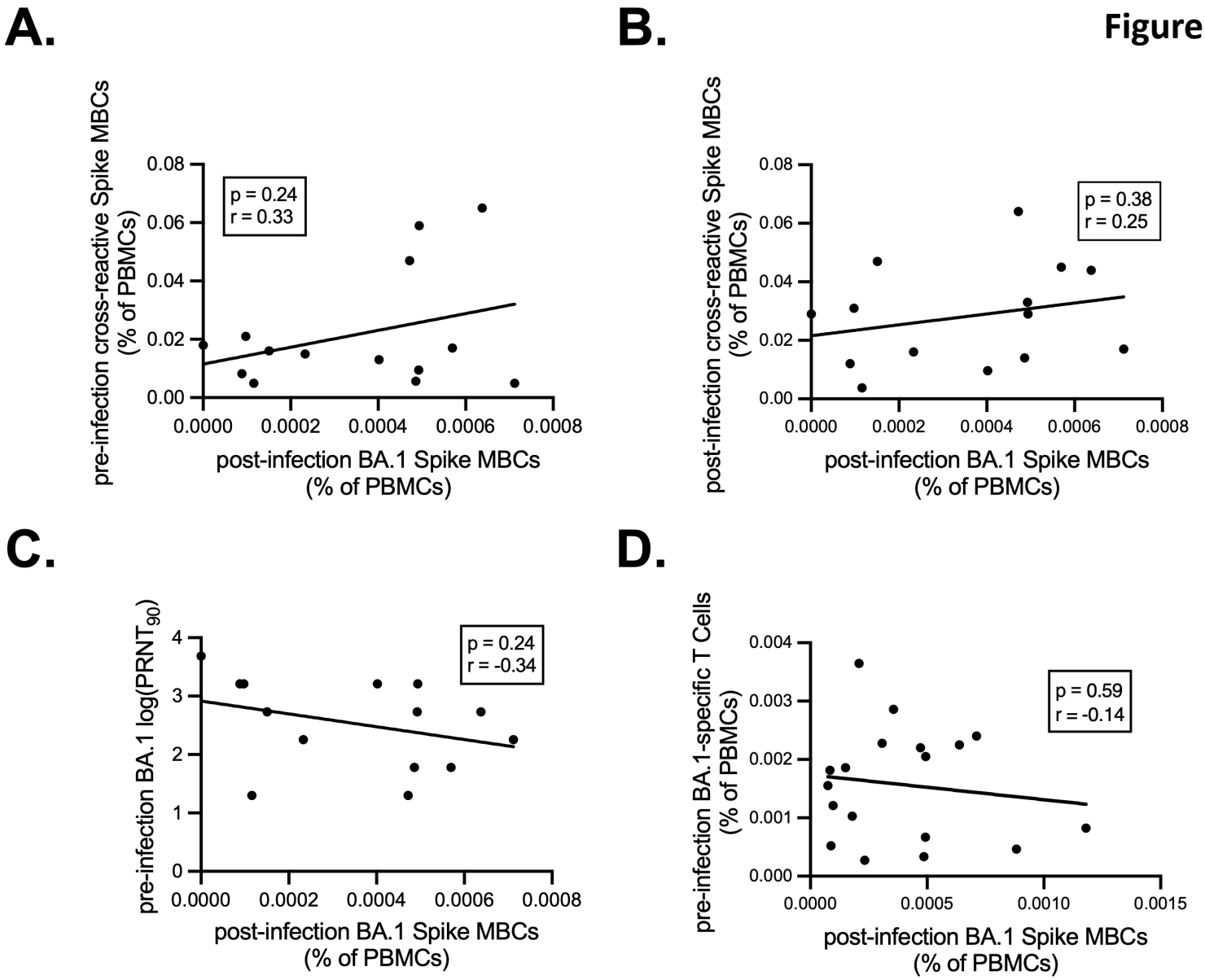
A.
pre-infection cross-reactive Spike MBCs (% of PBMCs)
0.08
0.06
0.04
0.02
0.00
p = 0.24
r = 0.33
0.0000
0.0002
0.0004
0.0006
0.0008
post-infection BA.1 Spike MBCs (% of PBMCs)
B.
post-infection cross-reactive Spike MBCs (% of PBMCs)
0.08
0.06
0.04
0.02
0.00
p = 0.38
r = 0.25
0.0000
0.0002
0.0004
0.0006
0.0008
post-infection BA.1 Spike MBCs (% of PBMCs)
C.
pre-infection BA.1 log(PRNT90)
4
3
2
1
0
p = 0.24
r = -0.34
0.0000
0.0002
0.0004
0.0006
0.0008
post-infection BA.1 Spike MBCs (% of PBMCs)
D.
pre-infection BA.1-specific T Cells (% of PBMCs)
0.004
0.003
0.002
0.001
0.000
p = 0.59
r = -0.14
0.0000
0.0005
0.0010
0.0015
post-infection BA.1 Spike MBCs (% of PBMCs)

1270 **Figure 7. Correlations of pre-infection and post-infection BA.1-specific antibody,**
1271 **T and B cell responses. (A)** Correlation of pre-infection cross-reactive Spike MBCs
1272 (calculated as in Figure 5C) plotted against the frequency of post-infection BA.1 Spike
1273 MBCs (calculated as in Figure 5C) in individuals that experienced a post-vaccination
1274 BA.1 infection. Pearson correlation analysis was performed. Pre-infection blood draws
1275 were taken on average 87.6 days before infection and post-infection draws were taken
1276 an average of 38.3 days after infection. Individuals that received a vaccine after the pre-
1277 infection draw were excluded from analysis. **(B)** Correlation of post-infection cross-
1278 reactive Spike MBCs (calculated as in Figure 6B) plotted against the frequency of post-
1279 infection BA.1 Spike MBCs (calculated as in Figure 5C) in individuals that experienced a
1280 post-vaccination BA.1 infection. Pearson correlation analysis was performed. **(C)**
1281 Correlation of pre-infection BA.1 neutralizing antibody titer (calculated as in Figure 4a)
1282 plotted against post infection BA.1 Spike MBCs (calculated as in Figure 5c) in
1283 individuals that experienced a post-vaccination BA.1 infection. Pearson correlation
1284 analysis was performed. **(D)** Correlation of pre-infection BA.1 Spike-specific T cells as
1285 measured by IFNγ ELISPOTs plotted against post-infection BA.1 Spike MBCs in
1286 individuals that experienced a post-vaccination BA.1 infection. Pearson correlation
1287 analysis was performed.
1288
1289

Figure S1

A.

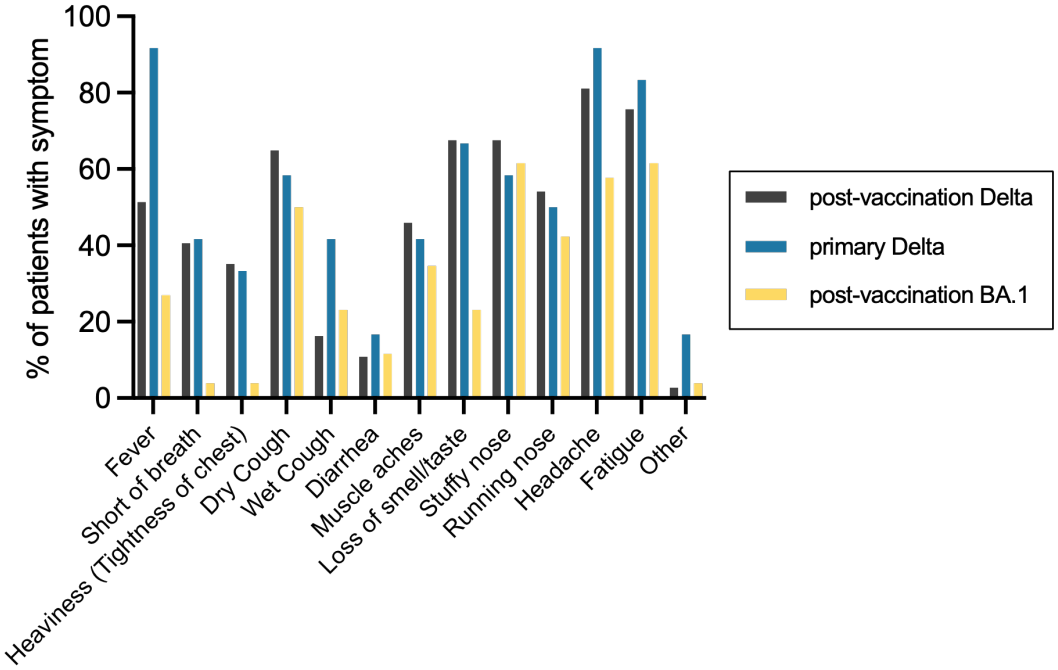
% of patients with symptom
100
80
60
40
20
0
Fever
Short of breath
Heaviness (Tightness of chest)
Dry Cough
Wet Cough
Diarrhea
Muscle aches
Loss of smell/taste
Stuffy nose
Running nose
Headache
Fatigue
Other
post-vaccination Delta
primary Delta
post-vaccination BA.1

B.

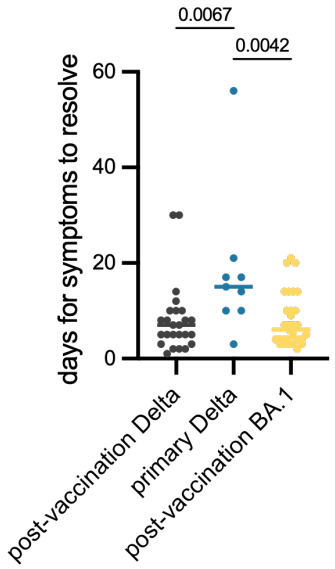
0.0067
0.0042
days for symptoms to resolve
60
40
20
0
post-vaccination Delta
primary Delta
post-vaccination BA.1

1290 **Figure S1. Test All, Test Smart (TATS) symptom report. (A)** Percentage of
1291 individuals from each TATS cohort that reported experiencing various respiratory/cold
1292 symptoms in study entry survey. **(B)** Reported days until symptoms resolved for each
1293 TATS cohort. Two-sided P values from t-test statistics were calculated for pairwise
1294 differences using one-way ANOVA. Post hoc testing for multiple comparisons between
1295 draws was performed using Tukey's multiple comparisons test. P values greater than
1296 0.05 are not depicted.
1297

Figure S2

A.

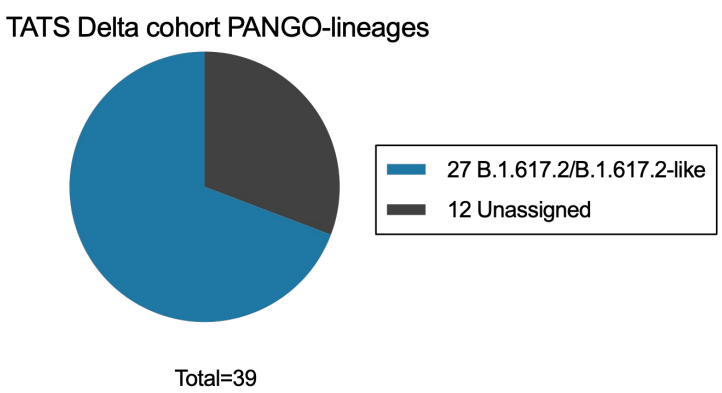
TATS Delta cohort PANGO-lineages
27 B.1.617.2/B.1.617.2-like
12 Unassigned
Total=39

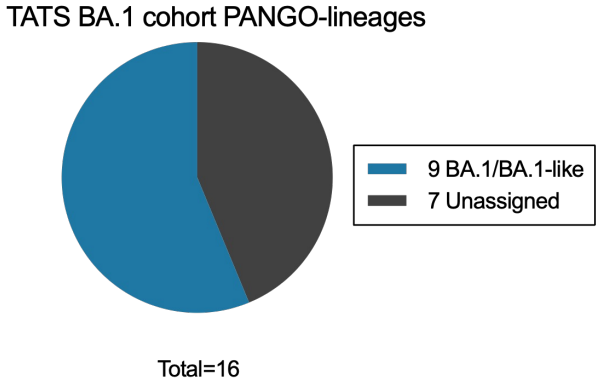
TATS BA.1 cohort PANGO-lineages
9 BA.1/BA.1-like
7 Unassigned
Total=16

B.

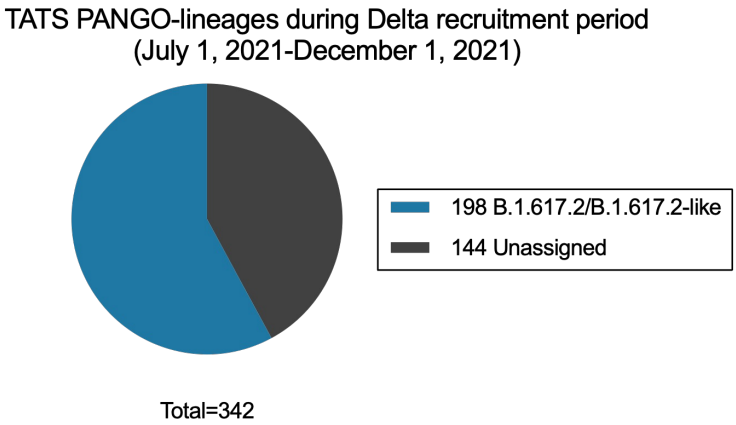
TATS PANGO-lineages during Delta recruitment period
(July 1, 2021-December 1, 2021)
198 B.1.617.2/B.1.617.2-like
144 Unassigned
Total=342

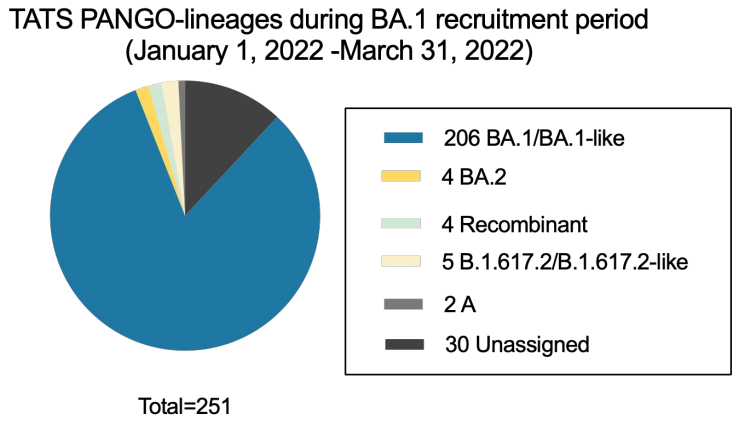
TATS PANGO-lineages during BA.1 recruitment period
(January 1, 2022 -March 31, 2022)
206 BA.1/BA.1-like
4 BA.2
4 Recombinant
5 B.1.617.2/B.1.617.2-like
2 A
30 Unassigned
Total=251

1298 **Figure S2. PANGO-lineage assignments from TATS PCR positive individuals. (A)**
1299 Delta or BA.1 PANGO-lineage assignments after SARS-CoV-2 viral amplicon
1300 sequencing (Integrated DNA Technologies). Unassigned sequences could not be
1301 assigned to a PANGO-lineage due to insufficient viral RNA recovery and low sequence
1302 coverage. **(B)** PANGO-lineage assignments of all TATS samples submitted during the
1303 period of Delta cohort recruitment, July 1, 2021-December 1, 2021 (left panel) or during
1304 the period of BA.1 cohort recruitment, January 1, 2022-March 31, 2022 (right panel).
1305 Unassigned sequences could not be assigned a lineage due to insufficient viral RNA
1306 recovery and low sequence coverage.

Figure S3

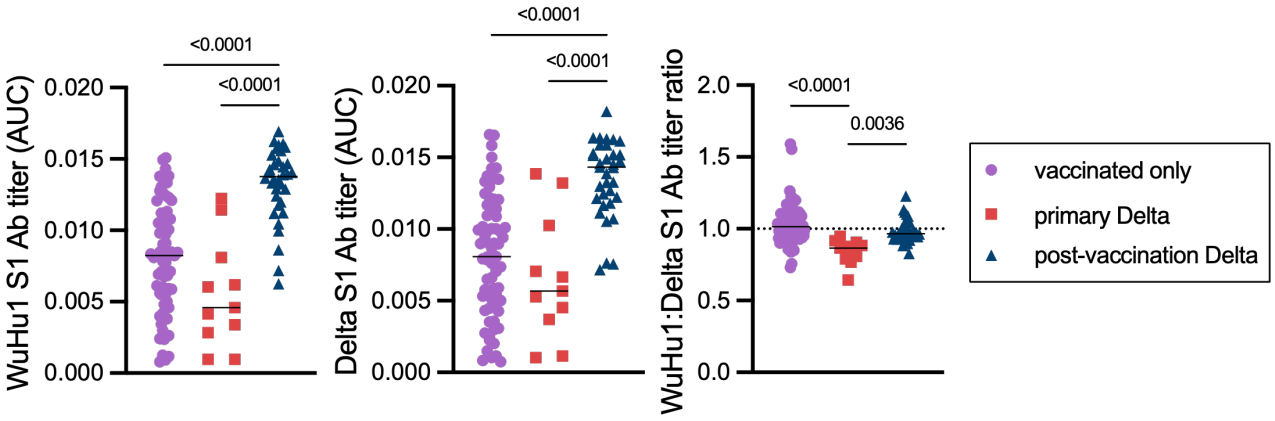
WuHu1 S1 Ab titer (AUC)
0.020
0.015
0.010
0.005
0.000
<0.0001
<0.0001
Delta S1 Ab titer (AUC)
0.020
0.015
0.010
0.005
0.000
<0.0001
<0.0001
WuHu1:Delta S1 Ab titer ratio
2.0
1.5
1.0
0.5
0.0
<0.0001
0.0036
vaccinated only
primary Delta
post-vaccination Delta

1307 **Figure S3. Primary and recall antibody responses to Wuhan and Delta strains of**
1308 **SARS-COV-2.** Quantitative titers of WuHu1- and Delta S1-specific antibodies. Serum
1309 was initially diluted 1:60, serially diluted 1:3, assessed by ELISA for binding to the listed
1310 antigens, and area under the curve (AUC) values were calculated. Each symbol
1311 represents an individual. WuHu1 AUC values were divided by their Delta AUC titer in
1312 the same individual to calculate a WuHu1:Delta S1 ratio in the rightmost panel. Two-
1313 sided P values from t-test statistics were calculated for pairwise differences using one-
1314 way ANOVA. Post hoc testing for multiple comparisons between draws was performed
1315 using Tukey's multiple comparisons test. P values greater than 0.05 are not depicted.
1316
1317
1318
1319

Figure S4

primary Delta

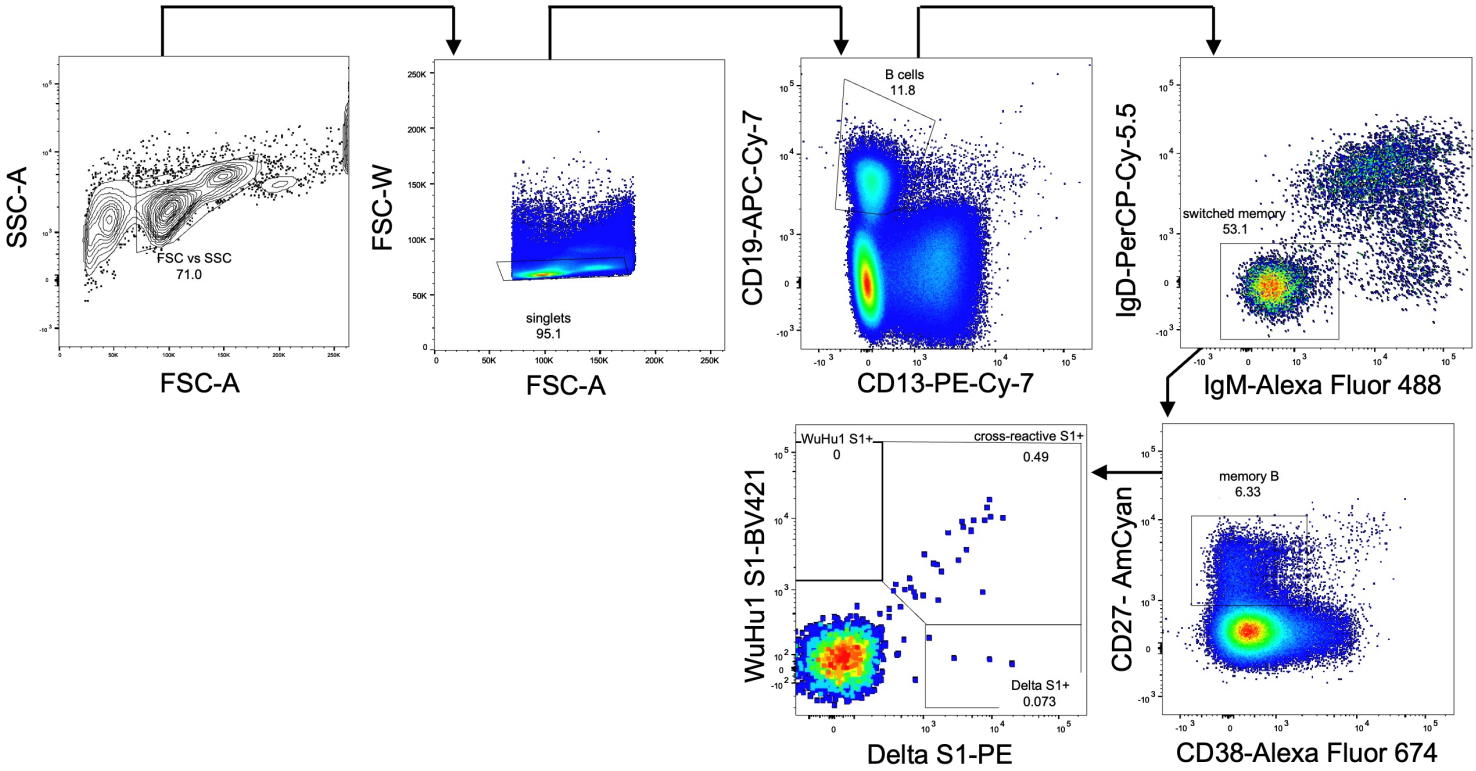

post-vaccination Delta

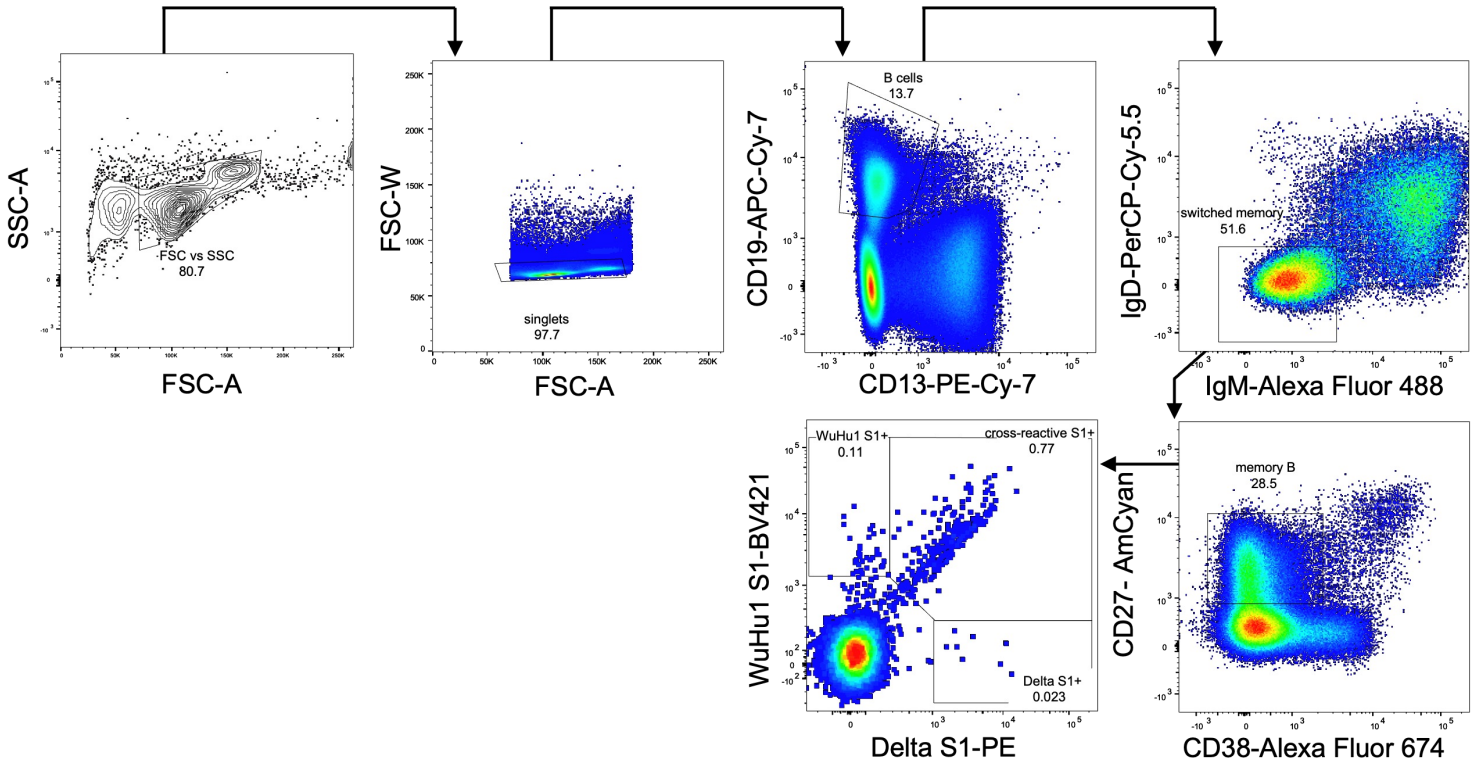

1320 **Figure S4. Flow cytometric gating strategy with Delta S1 and WuHu1 S1**

1321 **tetramers.** Examples of a sample from a primary Delta infection (top) and post-

1322 vaccination Delta infection (bottom) are shown.

1323

Figure S5

A.

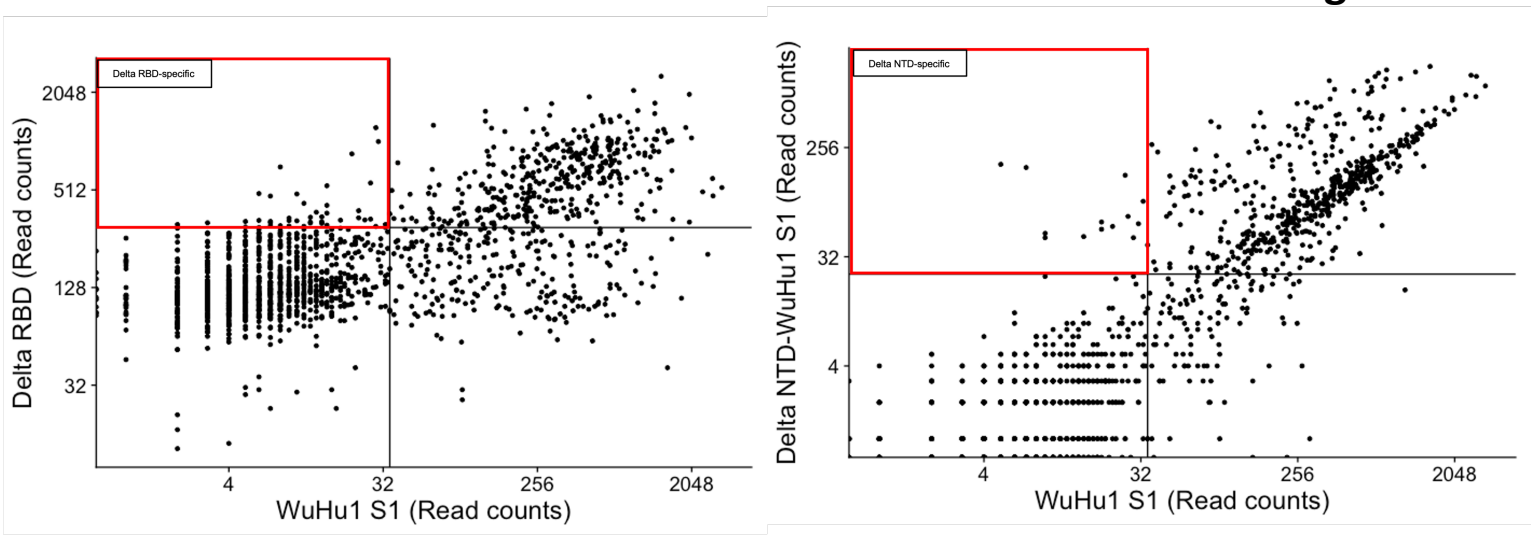

B.

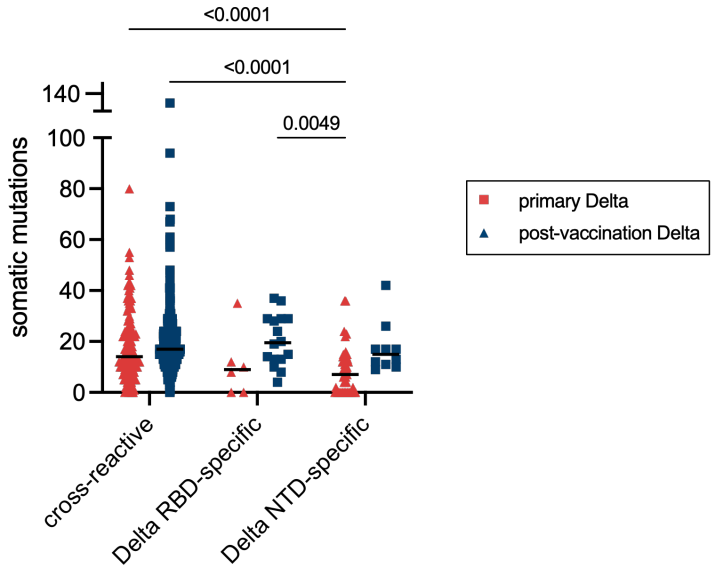

C.

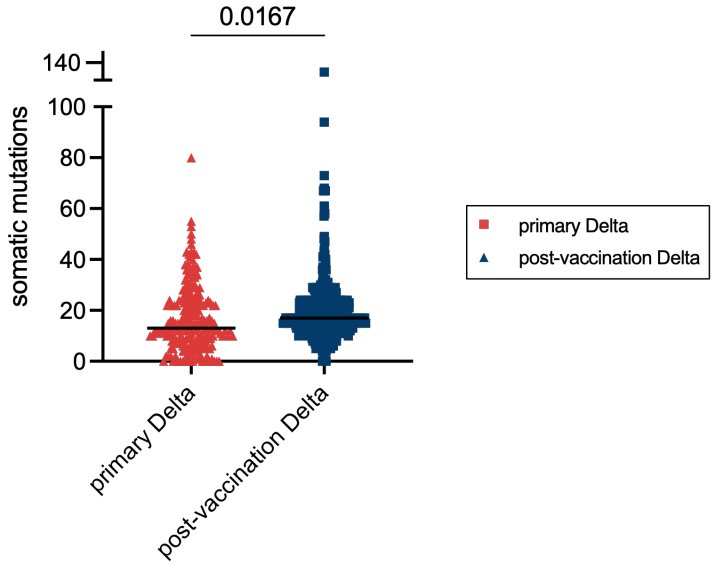

1324 **Figures S5. LIBRA-seq analysis in primary and post-vaccination Delta infections**
1325 **and quantification of somatic mutations. (A)** A chimeric protein (Delta NTD-WuHu1
1326 S1) was generated in which Delta NTD mutated epitopes (T19R, G142D, E156-, F157-,
1327 R158G) were incorporated into the otherwise WuHu1 S1 backbone. Quantification of
1328 Delta RBD-specific **(left)** and Delta NTD-specific memory B cells **(right)** in individuals
1329 that experienced a post-vaccination Delta infection. Delta RBD-specific cells were
1330 classified by cells that had Delta RBD read counts of greater than 300 and WuHu1 S1
1331 read counts of less than 35. Delta NTD-specific cells were classified by cells that had
1332 Delta NTD-WuHu1 S1 read counts of greater than 23 and WuHu1 S1 read counts of
1333 less than 35. Read count thresholds to determine positivity were set using samples in
1334 which cells lacking Spike-binding specificities were sorted and sequenced. Plots are
1335 concatenated from ten individuals. **(B)** Somatic mutations were calculated using the
1336 observedMutations command in the Shazam Immcantation package in R. Specificities
1337 of cells are determined using the same cutoffs described in **Figure S3A and 3D. (C)**
1338 Quantification of somatic mutations of all Spike specific cells subjected to scRNAseq
1339 from either ten primary or post-vaccination Delta infections.
1340
1341
1342
1343
1344

α-Nucleocapsid 1:60 Titer

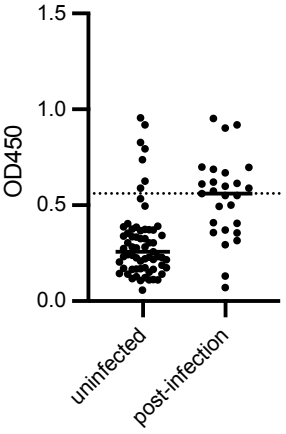

Figure S6

1345 **Figure S6. anti-Nucleocapsid titers in uninfected individuals.** Individuals with α-
1346 Nucleocapsid titers of greater than 0.6 at a1:60 serum dilution were considered
1347 previously infected and excluded from the study.
1348
1349

Figure S7

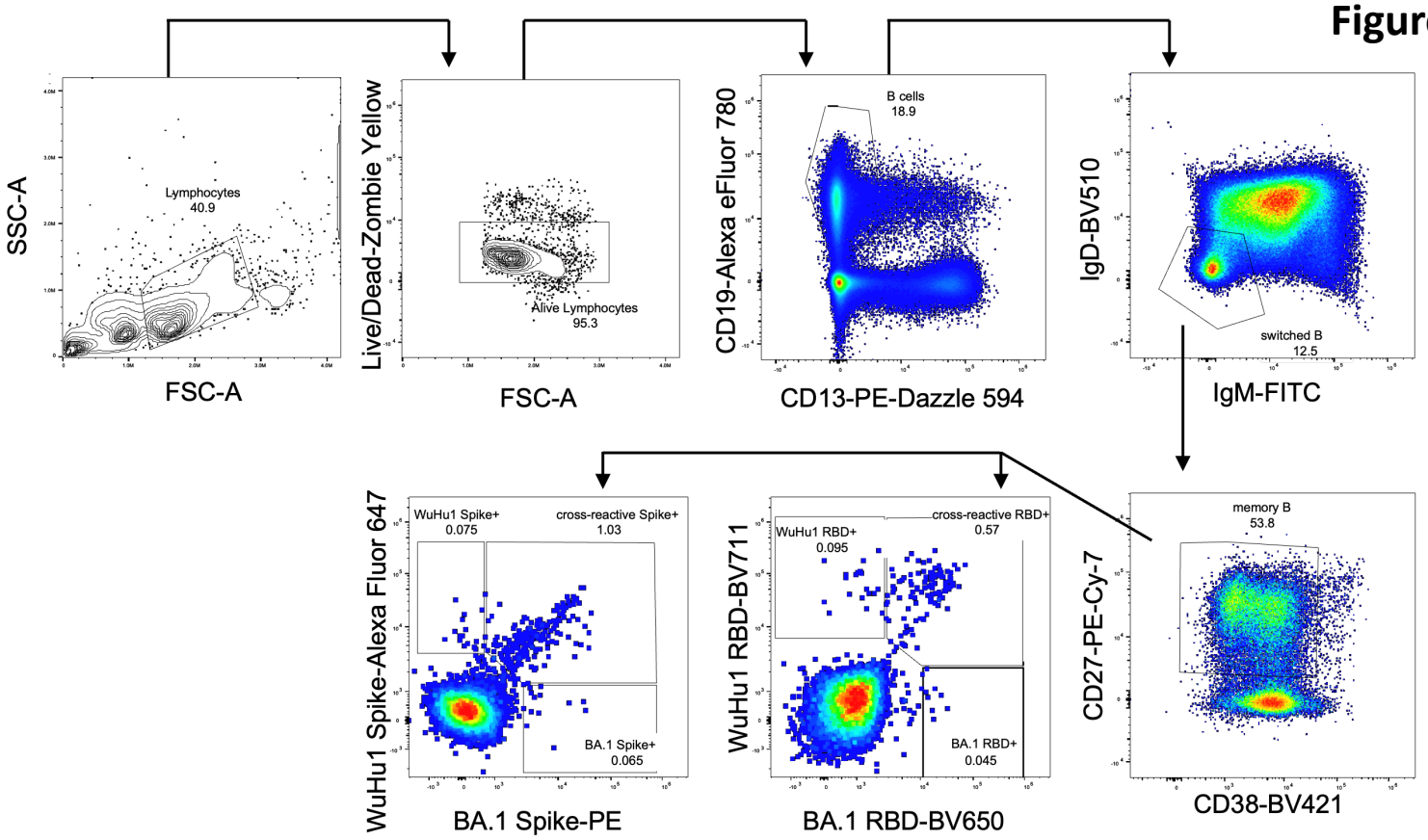
SSC-A
FSC-A
Lymphocytes
40.9
Live/Dead-Zombie Yellow
FSC-A
Alive Lymphocytes
95.3
CD19-Alexa eFluor 780
CD13-PE-Dazzle 594
B cells
18.9
IgD-BV510
IgM-FITC
switched B
12.5
WuHu1 Spike-Alexa Fluor 647
BA.1 Spike-PE
WuHu1 Spike+
0.075
cross-reactive Spike+
1.03
BA.1 Spike+
0.065
WuHu1 RBD-BV711
BA.1 RBD-BV650
WuHu1 RBD+
0.095
cross-reactive RBD+
0.57
BA.1 RBD+
0.045
CD27-PE-Cy-7
CD38-BV421
memory B
53.8

1350 **Figure S7. Flow cytometric gating strategy with BA.1 RBD, BA.1 Spike, WuHu1**

1351 **RBD and WuHu1 Spike tetramers.** An example of a sample from a post-vaccination

1352 BA.1 infection is shown.

1353

1354

Figure S8

A.

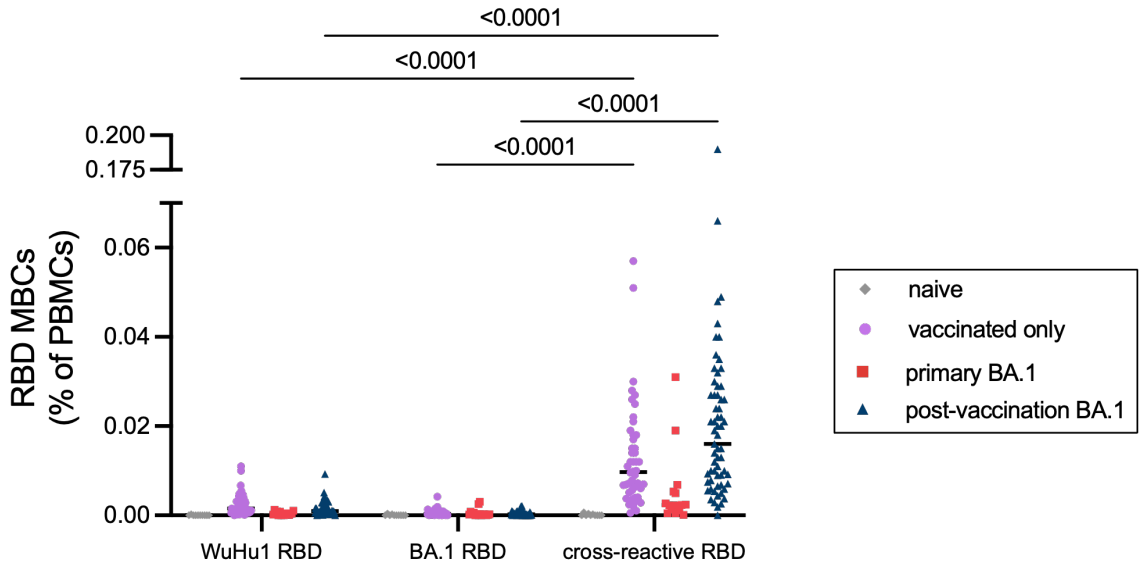
RBD MBCs
(% of PBMCs)
0.200
0.175
0.06
0.04
0.02
0.00
<0.0001
<0.0001
<0.0001
<0.0001
WuHu1 RBD
BA.1 RBD
cross-reactive RBD
naive
vaccinated only
primary BA.1
post-vaccination BA.1

B.

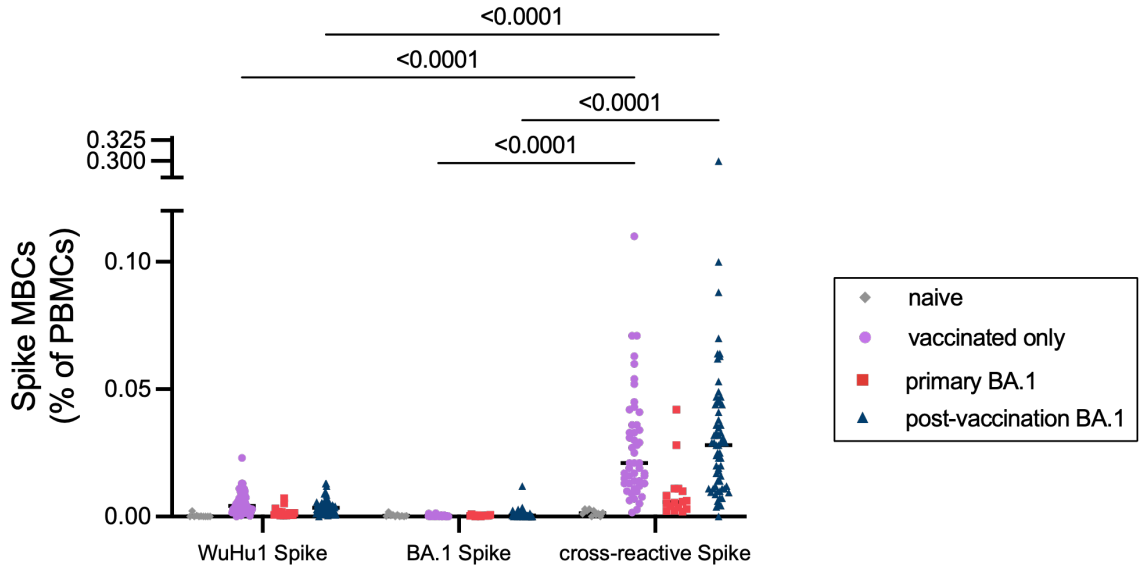
Spike MBCs
(% of PBMCs)
0.325
0.300
0.10
0.05
0.00
<0.0001
<0.0001
<0.0001
<0.0001
WuHu1 Spike
BA.1 Spike
cross-reactive Spike
naive
vaccinated only
primary BA.1
post-vaccination BA.1

1355 **Figure S8**. **WuHu1 and BA.1 Memory B cell flow cytometric quantification. (A)**
1356 Cells that bind both WuHu1 RBD and BA.1 RBD are annotated as cross-reactive RBD+,
1357 whereas cells that bind only WuHu1 RBD or BA.1 RBD are annotated as WuHu1 RBD+
1358 or BA.1 RBD+, respectively. Quantification of isotype-switched memory B cells as a
1359 percentage of total PBMCs for Wuhu1 RBD+, BA.1 RBD+ and cross-reactive RBD+
1360 specificities for each cohort of SARS-CoV-2 immune histories. Each symbol represents
1361 an individual. Two-sided P values from t-test statistics were calculated for pairwise
1362 differences using two-way ANOVA. Post hoc testing for multiple comparisons between
1363 draws was performed using Tukey's multiple comparisons test. P values greater than
1364 0.05 are not depicted. **(B)** Cells that bind both WuHu1 RBD and BA.1 Spike are
1365 annotated as cross-reactive Spike+, whereas cells that bind only WuHu1 Spike or BA.1
1366 Spike are annotated as WuHu1 Spike+ or BA.1 Spike+, respectively. Quantification of
1367 isotype-switched memory B cells for Wuhu1 Spike+, BA.1 Spike+ and cross-reactive
1368 Spike+ specificities for each cohort of SARS-CoV-2 immune histories. Each symbol
1369 represents an individual. Two-sided P values from t-test statistics were calculated for
1370 pairwise differences using two-way ANOVA. Post hoc testing for multiple comparisons
1371 between draws was performed using Tukey's multiple comparisons test. P values
1372 greater than 0.05 are not depicted.
1373

Table 1

	vaccinated only (statewide antibody testing initiative) (n=74)	primary Delta (n=12)	post-vaccination Delta (n=37)	vaccinated only (TATS) (n=62)	primary BA.1 (n=69)	post-vaccination BA.1 (n=62)
Age Mean (s.d.)	38.0 (32.0, 54.0)	21.9 (20.2, 40.7)	23.3 (18.6, 65.8)	31.9 (18.6, 65.0)	44 (25, 62)	40 (19, 71.5)
Sex						
Male	22 (32%)	5 (42%)	8 (22%)	24 (39%)		24 (39%)
Female	52 (68%)	7 (58%)	29 (78%)	37 (60%)		34 (55%)
Prior COVID infection						
Yes		12 (100%)	37 (100%)		69 (100%)	64 (100%)
No	74 (100%)					
Time since COVID infection		67.5 days (32, 99.3)	71.5 days (48.5, 89.5)		40 days (31, 44.5)	54.4 days (34.5, 71)
paired pre- and post- infection samples					10	21
Time from vaccination to pre- infection draw						138 (32.5, 217)
Time from pre- infection draw to infection					73.3 days (30, 99)	112 days (33, 187)
Time from infection to post- infection draw					42.7 days (29.5, 47.5)	44.8 days (34, 49.3)
COVID Vaccination	37	0	37	62	0	62
# of shots						
2	37 (100%)		37 (100%)	16 (26%)		13 (20%)
3				46 (74%)		15 (23%)
4						3 (5%)
time since vaccination	135.6 days (126, 270)		273.9 days (56, 317)	176.0 days (113.5, 188)		192.2 days (107, 302.3)

1374 **Table 1. Characteristics of cohorts**

1375 Interquartile range (IQR) is listed in parentheses unless otherwise stated in the table.

1376